Granular Matter (2015) 17:231–252
DOI 10.1007/s10035-015-0556-2

ORIGINAL PAPER

Computational modeling of the dynamics and interference effects of an erosive granular jet impacting a porous, compliant surface

Debanjan Mukherjee · Tarek I. Zohdi

Received: 19 February 2014 / Published online: 13 March 2015

Abstract The general problem of a loosely flowing erosive granular jet undergoing impact with a compliant surface is common in many manufacturing processes, and also in the operating environment of a variety of machine parts. This paper presents a three-dimensional, collision-driven discrete particle simulation framework for investigating the dynamics of a jet of erosive particles impacting a surface with a specified porosity and compliance. The framework is capable of handling repeated collisions between incoming particles and rebounding particles, and between particles and surfaces. It is also capable of performing a coupled simultaneous calculation of sub-surface stresses in the material, assuming a certain porosity. Well illustrated numerical examples are presented with detailed analysis for investigations on the mechanics and energetics of the interfering collisions in eroding jets close to the target surface, on the effect of such interference on the material erosion, and on the evolving stress levels and potential damage zones under the action of impact. Particularly, the assumption of considering first-order collisions between oncoming and rebounding jet particles is re-examined. The influence of repeated collisions on energy transferred to the surface was found to be significant under conditions which involves high particle numbers or fluxes, and also high degrees of inelasticity. The overall trends for parametric variations were found to be in accordance with reported trends in the literature.

Keywords Granular jet · Solid particle erosion · Collisions · Discrete element method · Interference effect

D. Mukherjee (✉) · T. I. Zohdi
Department of Mechanical Engineering, University of California, Berkeley, Berkeley, CA, USA
e-mail: debanjan@berkeley.edu

T. I. Zohdi
e-mail: zohdi@me.berkeley.edu

1 Introduction and background

In this work we focus on the general problem of a loosely flowing erosive granular jet undergoing impact with a compliant surface. This is a problem of interest in many industrial applications involving solid particle erosion, where durability of an engineered coating against erosive wear is to be investigated. This is also an important aspect for a range of industrial processes such as shot peening, blast cleaning, and abrasive finishing. The central idea behind all these processes is to accelerate a stream of particles and launch the stream towards a target surface. The general problem of erosive material removal due to a particle impact has been addressed in the classical works by Finnie [17], Bitter [5], and Hutchings et al. [26] amongst others. In all such investigations, the impact energy carried by the particle, the impingement angle, and particle dimensions and properties were correlated with measured values of eroded material for a single particle impact. In a recent work, Oka et al. [40] extend this idea to provide a more generalized correlation equation for predicting erosive wear. Interestingly, the trends in erosive wear observed from impact due to a stream of particles are somewhat different as compared to individual particle impact—as reported by Uemois and Kleis [48], who commented on a non-linear dependence of erosion rate on mass concentration of impacting particle streams. The observed maximum wear for single particle impacts would be at normal incidence, while that for a flowing stream of particles was found to be at an intermediate angle. While similar observations have been made by other investigators in the field, the complicated dependence of the behavior of the impacting stream on a wide range of parameters make it difficult to construct a predictive model for the same.

As the particles impacting the surface reflect back and start interacting with the oncoming stream of particles, the

impact energy due to the oncoming particles get significantly altered. Andrews and Horsfield [2] have presented a calculation of collision frequencies amongst particles in the vicinity of a target surface, and correlated those with observed collisions from a sand-blasting experiment. A similar analysis has been presented in the work by Anand et al. [1], where a simple model for calculating the fraction of non-colliding particles reaching the target surface was presented. Their work was based on the assumption of only first-order collisions between incoming and reflected particles, and any particle having collided with the surface was assumed to not affect the erosion process again. Using the model, an exponential dependence of erosion rate on flux of erosive particles impacting the surface was obtained. Both these models make a range of assumptions regarding the dynamics of the colliding system of eroding particles. In a more recent work, Burzynski and Papini [7] provide a comparative analysis of the models, and extended the derivation to include a broader range of parameters. This was further modified in a later, more recent work by Burzynski and Papini [8] where non-uniform spatial distribution of particles, and their velocities were also included. The analysis of the interference effect was also performed using a three-dimensional event-driven particle dynamics simulation framework developed by Ciampini et al. [13,14]. In this work, a broad range of parametric studies were presented on the amount of power arriving at the target surface due to the particle jet in the presence of interfering collisions—the conclusions being further advanced in their subsequent works (for example, see Gomes-Ferreira et al. [19]). The computer-model incorporated a broader range of system parameters and stream geometries, and a detailed discussion of the implications of these system parameters on erosive wear was provided as well. Experimental investigations using a gas-blast apparatus that addresses the issue of mass flux in erosive particle jets has been presented by Shipway and Hutching [45]. In a similar work Oka et al. [39] have presented experimental data on flux effects in sand-blasting applications.

The broad range of available data demonstrate a strong dependence of erosion performance on the interference effect. While available models and simulation frameworks mentioned herein have been able to address many questions related to the mechanics of the interfering collisions, the complex nature of the repeated collisions between the oncoming and reflected particles, and repeated collisions between a particle and the target surface (owing to interactions with the oncoming stream) have not been taken into account. In Ciampini et al. [14], the particle collisions have also been assumed to be frictionless. This was shown to have minor effect on the system performance at moderate fluxes, however in general one cannot assume that to be the case for a broader range of particle mass-flux or number densities—since with repeated collisions, the frictional energy losses can end up becoming significant. Furthermore, there has not been much attempts to create computer simulation models that can interface the dynamics of the particle stream to calculating stresses within the material continuum of the target surface. Individual projectile impacts on a target surface have been studied in much computational detail using finite element method in the works by Ramanujam and Nakamura [43], Camacho and Ortiz [9], and Chen et al. [11] amongst others. However, detailed sub-surface stress calculations coupled with simultaneous multi-particle impacts have not received such wide attention. Insights into the transformation of the energy contained by the impacting stream into sub-surface stresses is valuable for understanding process details—for example, sub-surface stress levels in shot-peening. Interfacing such detailed numerical models for the sub-surface material with a discrete particle simulation will end up becoming a computationally intensive task.

The focus of the present work is to illustrate the development of a computer simulation framework based on a three-dimensional discrete element based model to simulate the impact of a stream of loosely flowing particles (of varying particle number densities) upon a compliant surface having a porous micro-structure. The framework developed will not be based on any assumptions on the number of collisions between particles, or between particle and target surface—thereby allowing for capturing repeated collisions and their effect on the performance of the erodent particles. The applications of interest involve highly inertial particles accelerated to high velocities and shot towards the target surface, with particle densities being much higher compared to the surrounding gas. The particle momentum response time-scale is therefore much higher compared to the time-scale within which the particle stream interacts with the target surface. Thus the surrounding air/gas plays a minimal role given the high inertia and momentum, and gas–particle interactions have been neglected in the study. The framework will also include a coupled calculation of sub-surface stresses using simple estimates obtained from a superposition of individual particle impact loads. This allows for a visualization of the time-varying sub-surface stress distribution during the course of the impact of the stream. The organization of the paper is as follows: Sect. 2 describes the models for particle–particle and particle–surface contact interactions, and models for stress estimation; Sect. 3 outlines the assembly of the simulation framework and resolves some implementation details; Sect. 4 presents sample simulation results depicting the jet dynamics for various configurations, the estimated sub-surface stresses and damage levels, and the role of the microstructure on the stress levels; Sect. 5 illustrates the utility of the framework in understanding various aspects of the interference effects for erosive jets; followed by some concluding remarks in Sect. 1. We remark here that the work presented in this paper is part of an ongoing effort towards

developing a research-purpose software simulation library for discrete particle simulations.

2 Modeling

2.1 A brief overview of contact interaction models

The principal governing physical interactions for the dynamics of the particle streams are the particle–particle and particle–surface contact interactions. Owing to the underlying rigidity of the individual particles that comprise the erosive streams, these systems are collisionally dominant. There exist a wide range of approaches for characterizing the force between contacting bodies, and a comprehensive review of all the approaches will be beyond the scope of the current work. The interested reader is referred to the classical work of Johnson [27], and the extensive reviews on contact force models presented by Poschel and Schwager [42], and Shafer et al. [44]. A commonly used approach is to characterize the contact force between two bodies based on a geometric overlap that characterizes the contact deformation. For two spherical bodies of radii R_1 and R_2 (located at $\mathbf{r}_1$ and $\mathbf{r}_2$ respectively), this overlap is easily estimated by $\delta_n = (R_1 + R_2) - \|\mathbf{r}_1 - \mathbf{r}_2\|$. Obviously for negative values for δ_n, there is no contact occurring between the two bodies—which forms a direct check for contact detection. Perhaps the most fundamental of these models is the Hertzian model for normal contact (see Hertz [24] and Johnson [27]), which relates the normal contact force magnitude to the normal contact overlap as:

$$f_n = \frac{4}{3}\sqrt{R}E^*\delta_n^{3/2} = K_n\delta_n^{3/2} \tag{1}$$

where $1/R = 1/R_1 + 1/R_2$, and the effective elasticity E^* is defined as $\frac{1}{E^*} = \frac{1-\nu_1^2}{E_1} + \frac{1-\nu_2^2}{E_2}$, where ν_1,ν_2 and E_1,E_2 denote the Poisson's ratio and elasticity of the contacting particles. Similar to Hertz's approach, Mindlin [31] proposed a model for the tangential compliance during elastic contact, from which the tangential force can be calculated using tangential overlap δ_t as:

$$f_t = 8r_c\left(\frac{2-\nu_1}{G_1} + \frac{2-\nu_2}{G_2}\right)^{-1}\delta_t = K_t\delta_t \tag{2}$$

where r_c is the radius of the contact region between the two bodies, and G_1,G_2 denote the shear modulus of the particles. Similar models have also been presented by Walton and Braun [52], Vu-Quoc and Zhang [50], Haff and Werner [20], Cundall and Strack [15], and Poschel and Schwager [42] amongst others. More recently, contact force models including plastic deformation effects have been presented by Vu-Quoc et al. [49], and Zhang and Vu-Quoc [55], where the force-based formulation presented in the former has been further validated experimentally in the work by Plantard and Papini [41]. The implementation of these models in a computer simulation framework for resolving the particle dynamics requires the numerical time-steps to be lesser than the total duration of the contact. While this is required for physically correct representations of systems with enduring contacts (with contact-durations comparable to the characteristic time-scales of the particle system), for collisionally dominant systems with non-enduring contacts of significantly small durations, this may lead to stringent requirements on the numerical time-step sizes.

Alternatively, a direct pairwise balance of linear and angular momenta for a collection of contacting particles can be used to derive an estimate of the contact forces. This approach has been used for flowing particulate media in the works of Zohdi et al. (see Zohdi [58], Arbelaez et al. [3], Arbelaez et al. [4], and Zohdi [59] for details). For applications involving dynamic systems of particles undergoing non-enduring contacts, this provides a theoretically consistent estimate of the contact interactions. Furthermore, this approach does not require an explicit force deformation relation to be evaluated and integrated over the duration of the contact—thereby relaxing the restrictions on the time-step sizes to be lesser than contact duration. Hence, for the present work a momentum balance formulation has been employed.

2.2 Particle–particle contact model

In order to outline the expressions for the forces obtained using a direct balance of momenta, we refer to the schematic representations of inter-particle and particle–surface contacts as presented in Fig. 1. For particle–particle collisions, we define normal vectors for the pairwise collisions as follows:

$$\hat{\mathbf{n}}_{ji} = \frac{\mathbf{r}_j - \mathbf{r}_i}{\| \mathbf{r}_j - \mathbf{r}_i \|} \tag{3}$$

where $\mathbf{r}_i$ denotes the center of mass position vector for particle i, and $\hat{\mathbf{n}}_{ij}$ can be defined similarly. Assuming the particles are idealized to be rigid (that is, any contact deformations that occur are neither permanent nor significant as compared to the particle dimensions), the velocities at the point of contact for particle i—denoted hereafter as $\mathbf{v}_{pi}$—can now be written as:

$$\mathbf{v}_{pi} = \mathbf{v}_i + \boldsymbol{\omega}_i \times (R_i\hat{\mathbf{n}}_{ji}) \tag{4}$$

where $\mathbf{v}_i$ and $\boldsymbol{\omega}_i$ denote the particle center of mass velocity, and angular velocity respectively, and $\mathbf{v}_{pj}$ can be defined similarly. The relative velocity at the point of contact can now be defined as $\mathbf{v}_{rel} = \mathbf{v}_{pj} - \mathbf{v}_{pi}$. Using the relative velocity at the contact point, the direction of tangential slip can be characterized by a unit vector $\hat{\mathbf{t}}_{ij}$, as follows:

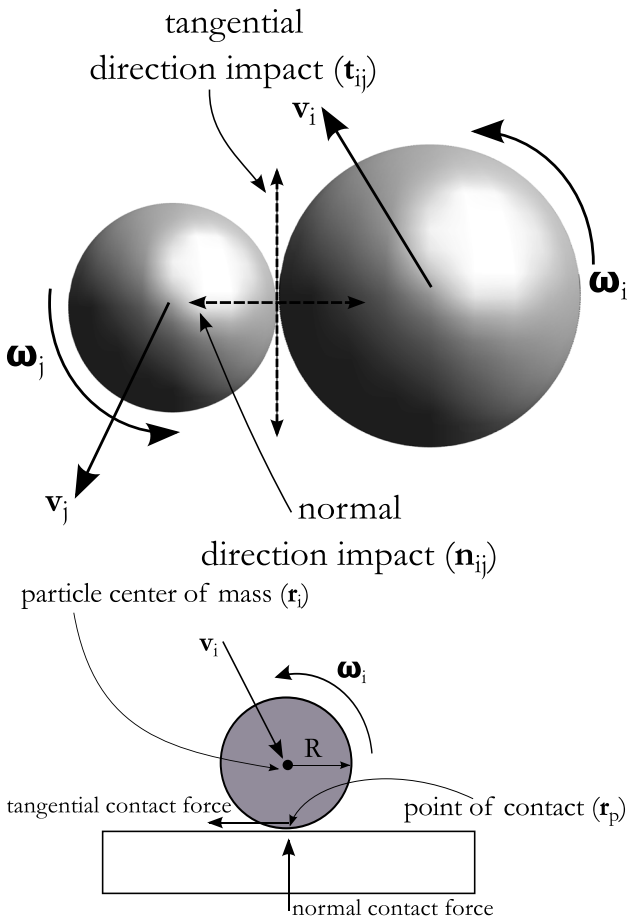

Fig. 1 Schematic of a typical particle–particle contact configuration (*top*) and particle–surface contact configuration (*right*) used to derive the collisional interactions using a balance of linear and angular momenta

$$\hat{\mathbf{t}}_{ij} = \frac{\mathbf{v}_{rel} - (\mathbf{v}_{rel} \cdot \hat{\mathbf{n}}_{ij})\hat{\mathbf{n}}_{ij}}{\parallel \mathbf{v}_{rel} - (\mathbf{v}_{rel} \cdot \hat{\mathbf{n}}_{ij})\hat{\mathbf{n}}_{ij} \parallel} \tag{5}$$

Assuming that the particles undergo collision over the interval $[t, t + \delta t]$, the pairwise linear momentum balance for the colliding particles over this collision duration δt can now be written as:

$$m_i \mathbf{v}_i(t + \delta t) - m_i \mathbf{v}_i(t) = \langle \mathbf{F}_i^c \rangle \delta t + \langle \mathbf{F}_i^e \rangle \delta t \tag{6}$$

$$m_j \mathbf{v}_j(t + \delta t) - m_j \mathbf{v}_j(t) = \langle \mathbf{F}_j^c \rangle \delta t + \langle \mathbf{F}_j^e \rangle \delta t \tag{7}$$

where $\langle \mathbf{F}_j^c \rangle \delta t = \int_t^{t+\delta t} \mathbf{F}_i^c dt$, and $\langle \mathbf{F}_j^e \rangle \delta t = \int_t^{t+\delta t} \mathbf{F}_i^e dt$ denote the averaged impulse due to the forces over the collision duration, and $\mathbf{F}_i^c$ and $\mathbf{F}_i^e$ denote the contact force and external, non-contact forces acting on particle i respectively. Since the collision durations δt are assumed to be much smaller than the numerical time-step Δt (say), we assume that variations in δt amongst particles will have a negligible effect on the system dynamics. Hence all particle pairs are assumed to have the same δt. Additionally the vectors $\hat{\mathbf{n}}_{ij}$, and $\hat{\mathbf{t}}_{ij}$ are also assumed to be constant over this small duration. Note that these assumptions will be consistent for collisionally dominant particulate systems, but for systems with enduring contacts where the contact deformations are explicitly tracked over the contact duration, these would no longer be true. Hence the formulations presented here are suited for collisionally driven particulate systems as mentioned earlier.

While the contact deformations are assumed negligible, in reality the work done by the mechanical forces within the bulk of the contact particles owing to any inelastic deformations leads to a dissipation of energy. This inelastic effect needs to be included in the system dynamics, and can be accounted for using the restitution coefficient (e). Decomposing the overall contact event into a compression phase where particles approach each other, followed by a recovery phase where particles recede from each other, the restitution coefficient (e) can be defined as the ratio between the normal contact impulse during recovery phase to that during compression phase. Assuming further that the total contact force for the pairwise collision on particle i can be written as $\mathbf{F}_i^c = f_{ni}\hat{\mathbf{n}}_{ij} + f_{ti}\hat{\mathbf{t}}_{ij}$, and performing some algebra the total normal contact force can be written as follows:

$$\langle f_{ni} \rangle \delta t = \frac{1+e}{m_i + m_j}\left[m_i \langle F_{jn}^e \rangle_C \delta t_1 - m_j \langle F_{in}^e \rangle_C \delta t_1\right] - \frac{(1+e)m_i m_j}{m_i + m_j}\left[v_{in}(t) - v_{jn}(t)\right] \tag{8}$$

where we have $v_{in} = \mathbf{v}_i \cdot \hat{\mathbf{n}}_{ij}$, $v_{jn} = \mathbf{v}_j \cdot \hat{\mathbf{n}}_{ij}$, $\langle F_{jn}^e \rangle_C \delta t_1 = \int_t^{t+\delta t_1} \mathbf{F}_j^e \cdot \hat{\mathbf{n}}_{ij} dt$, and $\langle F_{in}^e \rangle_C \delta t_1 = \int_t^{t+\delta t_1} \mathbf{F}_i^e \cdot \hat{\mathbf{n}}_{ij} dt$. The interval $[t, t + \delta t_1]$ denote the compression phase of the collision duration, hence the subscript C is employed for the averaged impulses over the duration δt_1 as defined herein. Alternative derivations of restitution coefficients for discrete element simulations have also been presented by Brilliantov et al. [6], and Muller and Poschel ([33] and [35]) amongst other works. The contact impulse can now be plugged back in to the linear momentum balance equations to get the respective post collisional velocity updates as follows:

$$m_i v_{in}(t + \delta t) = m_i v_{in}(t) + \frac{1+e}{m_i + m_j}\left[m_i \langle F_{jn}^e \rangle_C \delta t_1 - m_j \langle F_{in}^e \rangle_C \delta t_1\right] - \frac{(1+e)m_i m_j}{m_i + m_j}\left[v_{in}(t) - v_{jn}(t)\right] + \langle F_{in}^e \rangle \delta t \tag{9}$$

$$m_j v_{jn}(t + \delta t) = m_j v_{jn}(t) - \frac{1+e}{m_i + m_j}\left[m_i \langle F_{jn}^e \rangle_C \delta t_1 - m_j \langle F_{in}^e \rangle_C \delta t_1\right] + \frac{(1+e)m_i m_j}{m_i + m_j}\left[v_{in}(t) - v_{jn}(t)\right] + \langle F_{jn}^e \rangle \delta t \tag{10}$$

For the tangential component of the contact impulses, the momentum balance in $\hat{\mathbf{t}}_{ij}$ [see Eq. (5)] can be used along with a Coulomb stick-slip criteria, to derive expressions for the impulse. The inherent discontinuity of the stick-slip law can lead to mathematical complications, thereby requiring rigorous numerical techniques to handle such a model within the rigid body assumption for contact force calculation. An extensive review of the techniques available can be found in Stewart [46]. The latest developments, as discussed in the review, incorporate the idea of impulsive forces in rigid body dynamics, as measures of distributions instead, and the idea of combining rigid body contact problems with an area of convex analysis called the linear complementarity problem (for mathematical foundations of the method see the text by Murty [36]). However, the implementation of such a formulation into the time-discretized motion equations for a system of particles can be a complex task, as discussed by Stewart [46]. For systems of flowing particles with non-enduring contacts the system behavior is not significantly dependent on the exact stick-slip nature of the contact friction, as opposed to more static, enduring contacts (see for example the discussion by Duran [16], and Poschel and Schwager [42]). Therefore, for the applications of interest in this paper, the exact determination of stick-slip friction in an impulse-momentum balance type contact formulation can be replaced by a simple regularization of the discontinuous Coulomb friction law. Such regularized friction models can lead to robust numerical methods for integrating the motion equations. Discussions on the models for regularized Coulomb friction can be found in the works by Oden and Pires [38], and by Wriggers [54], and in general, the friction force can be given by (for particle i):

$$\langle f_{ti} \rangle = \mu \mathcal{R}\left(v_{slip,t}\right) \parallel f_{ni} \parallel \tag{11}$$

where $v_{slip,t}$ is the tangential slip velocity between the particles at the point of contact which can be estimated as $v_{slip,t} = \mathbf{v}_{rel} \cdot \hat{\mathbf{t}}_{ij}$, and $\mathcal{R}\left(v_{slip,t}\right)$ is a regularization function that approximates the discontinuity of the stick-slip criteria. A commonly used form of the regularization function $\mathcal{R}$ can be given as follows:

$$\mathcal{R}_1\left(v_{slip,t}\right) = \begin{cases} -1 & \forall v_{slip,t} < -\epsilon \\ \frac{v_{slip,t}}{2\epsilon} & \forall -\epsilon \leq v_{slip,t} \leq \epsilon \\ 1 & \forall v_{slip,t} > \epsilon \end{cases} \tag{12}$$

where ϵ is a regularization parameter, and smaller values of this parameter lead to better approximations of the stick-slip friction law. The tangential velocity updates can now be given using the tangential component momentum balance as follows:

$$\begin{aligned} m_i v_{it}(t+\delta t) &= m_i v_{it}(t) + \mu \mathcal{R}\left(v_{slip,t}\right) \parallel f_n \parallel \delta t \\ &\quad + \langle F^e_{it} \rangle \delta t \end{aligned} \tag{13}$$

$$\begin{aligned} m_j v_{jt}(t+\delta t) &= m_j v_{jt}(t) - \mu \mathcal{R}\left(v_{slip,t}\right) \parallel f_n \parallel \delta t \\ &\quad + \langle F^e_{jt} \rangle \delta t \end{aligned} \tag{14}$$

In order to balance the angular momenta, we define a third unit vector $\hat{\mathbf{s}}_{ij} = \hat{\mathbf{n}}_{ij} \times \hat{\mathbf{t}}_{ij}$, to complete a triad. The total angular momentum balance can now be written in terms of components along $\hat{\mathbf{s}}_{ij}$ for the two bodies as follows:

$$\begin{aligned} I_i \omega_{is}(t+\delta t) &= I_i \omega_{is}(t) - R\langle f_t \rangle \delta t + \langle M_{is} \rangle \delta t \\ &= I_i \omega_{is}(t) - R\mu \mathcal{R}\left(v_{slip,t}\right) \parallel f_n \parallel \delta t \\ &\quad + \langle M_{is} \rangle \delta t \end{aligned} \tag{15}$$

$$\begin{aligned} I_j \omega_{js}(t+\delta t) &= I_j \omega_{js}(t) - R\langle f_t \rangle \delta t + \langle M_{js} \rangle \delta t \\ &= I_j \omega_{js}(t) - R\mu \mathcal{R}\left(v_{slip,t}\right) \parallel f_n \parallel \delta t \\ &\quad + \langle M_{js} \rangle \delta t \end{aligned} \tag{16}$$

where $\mathbf{M}_i, \mathbf{M}_j$ are external moments acting on the spheres, and $\langle Mis \rangle \delta t = \int_t^{t+\delta t} \mathbf{M}_i \cdot \hat{\mathbf{s}}_{ij} dt$.

2.3 Particle–surface contact model

The contact interactions between a particle and a surface can also be formulated using similar impulse-momentum balance formulation. Assuming the surface description is known to be in form of a mathematical representation $\mathcal{F}(x, y, z) = 0$, it is possible to define a normal vector to the surface by using the following definition (for the unit outward normal) $\hat{\mathbf{n}} = -\frac{\nabla \mathcal{F}}{\|\nabla \mathcal{F}\|}$. We consider a spherical particle approaching this surface, and denote the point of contact with subscript p, and center of mass with the subscript c (schematic shown in Fig. 1). If the surface velocity vector is known to be $\mathbf{v}_{surf}$, then the slip velocity at the point of contact can be obtained as:

$$\mathbf{v}_{slip} = \left(\mathbf{v}_p - \mathbf{v}_{surf}\right) - \left[\left(\mathbf{v}_p - \mathbf{v}_{surf}\right) \cdot \hat{\mathbf{n}}\right] \hat{\mathbf{n}} \tag{17}$$

following which, the direction of tangential slip can be defined as:

$$\hat{\mathbf{t}} = \frac{\mathbf{v}_{slip}}{\parallel \mathbf{v}_{slip} \parallel} \tag{18}$$

From Fig. 1 the generic form of the contact force acting on the particle can be now motivated to be $\mathbf{F}^c_i = f_n \hat{\mathbf{n}} - f_t \hat{\mathbf{t}}$. Starting from the balance of linear momentum for the particle over the contact duration and using the definition of restitution coefficient (e) as in the previous section, the final expression for the normal force can be estimated as follows:

$$\begin{aligned} \langle f_n \rangle \delta t &= \langle f_n \rangle_C \delta t_1 + \langle f_n \rangle_R (\delta t - \delta t_1) \\ &= (1+e)\left[m v_{surf,n} - m v_{cn}(t) - \langle F^e_n \rangle \delta t_1\right] \end{aligned} \tag{19}$$

Plugging the expression for the total contact impulse into the balance of linear momentum of the particle, the post impact

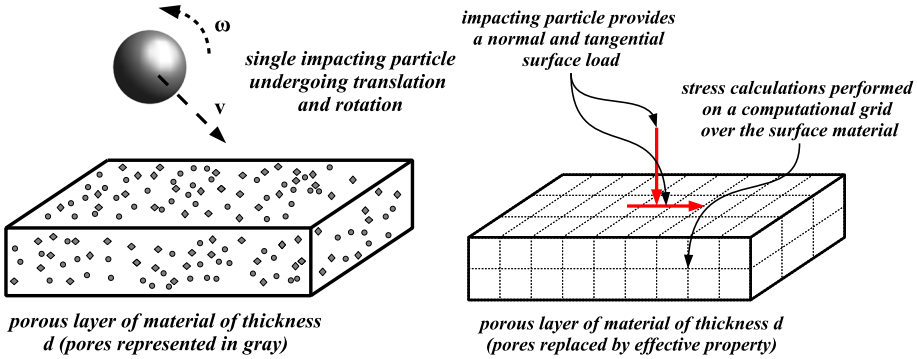

Fig. 2 A schematic representation of the translation of impact loads and material porosity into a simple stress-calculation framework over the material continuum (color figure online)

normal velocity of the particle can be obtained as follows:

$$v_{cn}(t+\delta t) = (1+e)v_{surf,n} - ev_{cn}(t) + \frac{1}{m}\langle F_n^e\rangle_R(\delta t - \delta t_1) - \frac{e}{m}\langle F_n^e\rangle_C \delta t_1 \tag{20}$$

The tangential force can be estimated using a regularized friction model analogous to the case of particle particle contact using Eq. (11). The tangential velocity updates can then be obtained again using Eq. (13), and the updates to the angular velocities due to the contact can be obtained using Eq. (15).

2.4 Stress estimates

The contact forces can be translated into stresses in the surface material, by considering the surface being impacted to be a semi-infinite half-space, and considering the contact forces to be applied surface tractions, as explained in the schematic in Fig. 2. This is a good abstraction for cases where the contact does not involve extensive deformations as compared to the dimensions of the surface—which is a reasonably good approximation for erosive wear of surfaces under impact by abrasive particles. Semi-analytical solutions for the sub-surface stresses obtained using Boussinesq potential functions for point and distributed tractions on a semi-infinite elastic half-space are used for the applied surface tractions. For the sake of a concise presentation the detailed expressions for the solutions for stress components are not outlined here but compiled in the Appendix. The interested reader is referred to Johnson [27] for the details of the derivation. A fully detailed analysis of the deformations and stresses would require a finite element type calculation over a discretized mesh of the bulk of the particle–surface combination—as found in Camacho and Ortiz [9] and more recently in Ramanujam and Nakamura [43]. The general form of the expressions for the stress components σ_{ij} at a sub-surface location $\bar{\mathbf{x}}$ due to contact at a location $\mathbf{x}_{con}$ with contact force $\mathbf{F}^c$ is as follows:

$$\sigma_{ij} = \sigma_{ij}\left(\bar{\mathbf{x}}; \mathbf{x}_{con}, \mathbf{F}^c, \text{material properties}\right) \tag{21}$$

This form can be used now to construct the stresses due to multiple impacts and at multiple locations within the material by superposition (see Fig. 2 for a schematic of a grid-based calculation for the same). We remark here, that in case a Hertzian type model is used for resolving the particle contact, instead of the impulse based model outlined here—similarly derived explicit expressions for Hertzian tractions distributed over the contact area between a sphere and a half-space will need to be employed (see Hamilton [21]).

2.5 Material properties of the porous layer

The presence of pores in the microstructure of the material layer will lead to the material properties of the layer be spatially variable parameters. An estimate of the material bulk and shear moduli is necessary for calculating surface and subsurface stresses, and damage, due to the impact by the particle stream. However, a direct numerical simulation to calculate the spatially varying material properties is a computationally expensive proposition. This is primarily because the underlying discretized computational mesh of the material layer has to resolve the microstructure at the individual pore level, leading thereby to an exceptionally fine mesh. Specifically for the coupled framework of dynamic translation of particle impact forces into stresses that is being proposed here, a fully discretized simulation for material properties therefore adds much computational overhead. Therefore, it is advantageous to use analytical estimates for the effective properties of the porous material layer as a first-order approximation. The central idea behind this is to use analytical, closed-form, expressions for the upper and lower bounds of the effective material properties, and then approximate the actual effective material property to be a combination of the bounds (see Zohdi [56,57]). For this work, we use the property bounds obtained from variational principles by Hashin and Shtrikman ([22,23]). For a two-phase material with volume fractions v_1, v_2, bulk moduli κ_1, κ_2, and shear moduli μ_1, μ_2 (with $\kappa_2 > \kappa_1$, and $\mu_2 > \mu_1$), the lower and upper bounds for the effective bulk modulus κ^* as given by Hashin and Shtrikman are as follows:

$$\kappa^{*,-} := \kappa_1 + \frac{v_2}{\frac{1}{\kappa_2-\kappa_1} + \frac{3(1-v_2)}{3\kappa_1+4\mu_1}} \tag{22}$$

$$\kappa^{*,+} := \kappa_2 + \frac{1-v_2}{\frac{1}{\kappa_1-\kappa_2} + \frac{3v_2}{3\kappa_2+4\mu_2}} \tag{23}$$

$$\kappa^{*,-} \leq \kappa^* \leq \kappa^{*,+} \tag{24}$$

and the lower and upper bounds for the shear modulus μ^* are as follows:

$$\mu^{*,-} := \mu_1 + \frac{v_2}{\frac{1}{\mu_2-\mu_1} + \frac{6(1-v_2)(\kappa_1+2\mu_1)}{5\mu_1(3\kappa_1+4\mu_1)}} \tag{25}$$

$$\mu^{*,+} := \mu_2 + \frac{1-v_2}{\frac{1}{\mu_1-\mu_2} + \frac{6v_2(\kappa_2+2\mu_2)}{5\mu_2(3\kappa_2+4\mu_2)}} \tag{26}$$

$$\mu^{*,-} \leq \mu^* \leq \mu^{*,+} \tag{27}$$

For isotropic microstructure with isotropic effective properties, these bounds are the tightest provided no additional micro-topological information is available. A reasonably good approximation of the overall effective property can now be constructed using a convex combination of the bounds as follows:

$$\kappa^* \approx \phi\kappa^{*,+} + (1-\phi)\kappa^{*,-} \tag{28}$$

$$\mu^* \approx \phi\mu^{*,+} + (1-\phi)\mu^{*,-} \tag{29}$$

where $\phi \in [0, 1]$. In order to incorporate porosity of the material layer as a micro structural variable, we assume that the material is effectively a multi-phase composite, with the pores and voids making up phase 1—such that $\kappa_1 = C\kappa_2$, and $\mu_1 = C\mu_2$, where C is a very small number. This can be plugged into Eqs. (22–26), and (28–29) to obtain the effective mechanical properties of the porous material. It was found from repeated numerical experimentation that the property estimates are insensitive to changes in the value of C beyond $\approx 10^{-4}$. Clearly then the porosity(p) is going to be given by $p = v_1$, and we can plug in $v_2 = 1 - p$ in Eqs. (22), (23), (25), and (26).

2.6 Damage equivalent stresses and a simple damage model

The characterization of damage due to particle erosion and material removal has received much attention from both experimental and modeling perspectives. The earlier works by Finnie [17] and Bitter [5] characterized a series of erosive wear phenomena, and for ductile and brittle materials, they outlined the different causes of erosive wear. In a later work on ceramic coatings, Nicholls et al. [37] further explored the characterization of erosive material loss from these coatings upon impact by particles. For brittle materials, Finnie [17] described the mechanics of crack induced damage and the propagation of circumferential ring cracks. For the current example, we incorporate a simplified damage criteria based on an appropriately defined equivalent stress. This is a non-local form of characterizing the potential damage a particle impact can induce and in order to do so, we define (as per the discussions presented in the work by Lemaitre and Desmorat [28]) the triaxiality function R_v as follows:

$$R_v = \frac{2}{3}(1+\nu) + 3(1-2\nu)\left(\frac{\sigma_{dil}}{\sigma_{vm}}\right)^2 \tag{30}$$

where σ_{dil} is the total dilatational stress, and σ_{vm} is the Von Mises effective stress. The term R_v indicates the three-dimensional distribution of the stresses, which is known to substantially influence the inelastic deformations leading to failure in a material. It relates to the strain energy density release rate (see Chaboche [10] and also Lemaitre and Desmorat [28] for details on the derivations) thereby providing a thermodynamic basis for utilizing such a criteria. The criteria for non-local damage can now be stated in terms of an equivalent stress σ_{eq} that can be written as:

$$\sigma_{eq} = \sigma_{vm}\sqrt{R_v} \geq \sigma_0 \tag{31}$$

where σ_0 is an effective stress threshold, and can be set to be the yield stress or ultimate stress depending on the kind of material. In order to use this equivalent stress to estimate the evolution of damage across the continuum of the material the following variable is defined:

$$\Pi = \frac{\sigma_{eq} - \sigma_0 + \parallel \sigma_{eq} - \sigma_0 \parallel}{2\sigma_0} \tag{32}$$

This variable is a non-dimensional measure of an indicator of damage initiation, and is zero for all cases where the equivalent stress is lesser than the critical. The potential damage at a certain location in the material continuum can be tracked by the number of times during the simulation that $\Pi > 0$—that is, by tracking the number of occurrences of high damage equivalent stresses at a location. Mathematically speaking, the damage model then can be given by:

$$\mathcal{D} = \sum_{grid} \mathcal{I}(\Pi > 0) \tag{33}$$

where $\mathcal{I}(\Pi > 0)$ is an indicator function whose value is unity if the argument condition holds true, and zero otherwise. The sum is done over a computational grid which discretizes a specified region of material.

2.7 Interfering collisions: a model problem with two particles

As we set out to discuss a detailed three-dimensional particle dynamics simulation framework, a simple model problem with two particles can be presented as a motivating example for quantifying the energetics of repeated collisions in particle streams. In a related study, Muller and Poschel

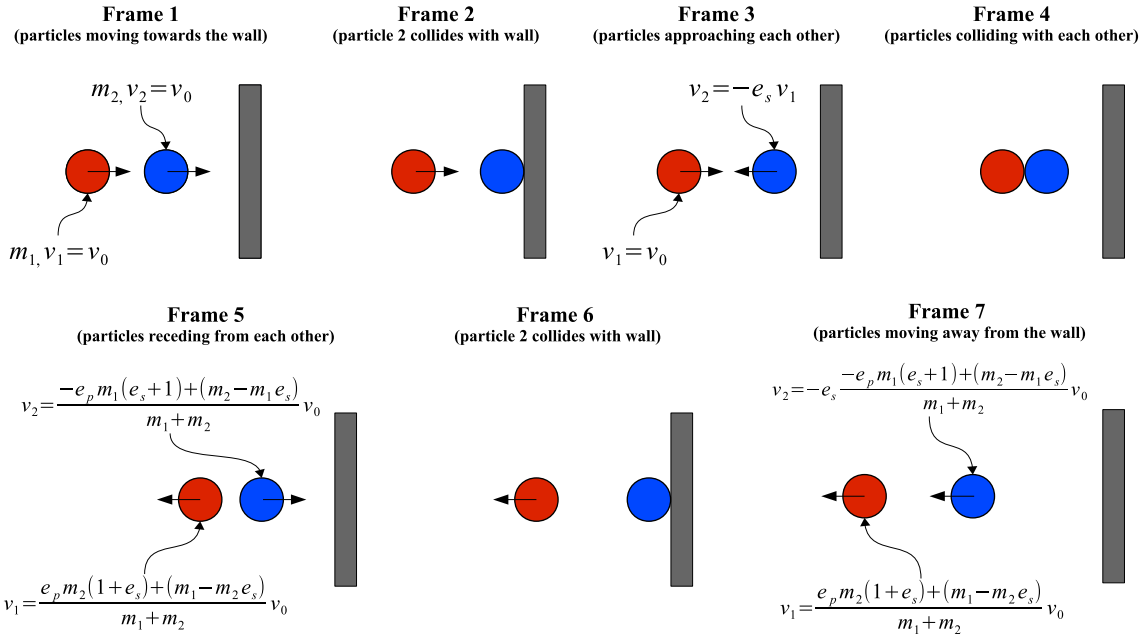

Fig. 3 Successive sequence of events during the collision of the model problem of two-particles approaching with a target surface (color figure online)

[34] have presented a calculation for repeated collisions of two spheres. Their discussions examined the instantaneous collision assumption central to choosing event-driven simulation models over force-based. However, for the present work, it is of interest to quantify the variations in energy loss, and imparted energy on the surface, with repeated collisions. For this purpose, we consider two particles approaching a target surface, and analyze the sequence of events as demonstrated in Fig. 3. The respective particle velocities can be calculated based on the particle–particle and particle–wall restitution coefficients as shown in the figure. The total energy loss in the event the particle collision interactions were not considered could now be easily quantified as $\Delta E_0 = \frac{1}{2}(m_1 + m_2)(1 - e_s^2)v_0^2$, with e_s being the particle–surface contact restitution coefficient. This is assuming that each particle collides with the surface only once and rebounds. The same energy difference, if quantified for the case with all the interactions included, will be as follows:

$$\begin{aligned}\Delta E^* = &\frac{1}{2}(m_1 + m_2)v_0^2 \\ &- \frac{m_1}{2}e_s^2\left[\frac{e_p m_2(v_0 + e_s v_0) - m_1 e_s v_0 + m_2 v_0}{m_1 + m_2}\right]^2 \\ &- \frac{m_2}{2}\left[\frac{-e_p m_1(e_s v_0 + v_0) + m_2 V_0 - m_1 e_s v_0}{m_1 + m_2}\right]^2\end{aligned} \tag{34}$$

where e_p denotes the particle–particle contact restitution coefficient. In the special case of equal masses, ΔE^* can be compared to the value ΔE_0 as follows:

$$\begin{aligned}\Delta E_0 - \Delta E^* = &\frac{mV_0^2}{8}\left[e_s^2(1 - e_s + e_p + e_s e_p)^2\right] \\ &+ \frac{mV_0^2}{8}\left[(1 - e_s - e_p - e_s e_p)^2\right] - mV_0^2 e_s^2\end{aligned} \tag{35}$$

Furthermore, if it is assumed that only first-order collisions are considered for quantifying the interactions, then the second collision of particle 1 with the surface will be rejected from the analysis, and referring to the energy difference as $\overline{\Delta E}$, we get the following (for particles of equal masses m):

$$\Delta E_0 - \overline{\Delta E} = mV_0^2\left[\frac{1}{4}\left[(1 - e_s)^2 + e_p^2(1 + e_s)^2\right] - e_s^2\right] \tag{36}$$

A comparison between these two cases can be now constructed by defining a non-dimensional ratio of the extent of initial energy of the particles that is lost during the entire event, for the case with all collisions included (α^*), and the case with only first-order collisions included ($\overline{\alpha}$) as follows:

$$\alpha^* = \frac{\Delta E_0 - \Delta E^*}{E_0}, \quad \overline{\alpha} = \frac{\Delta E_0 - \overline{\Delta E}}{E_0} \tag{37}$$

These ratios have been compared for varying particle–particle, and particle–surface restitution coefficients in Fig. 4, with the figure on the left being that for the special case when both the restitution coefficients have equal magnitudes. The figure indicates that the effect of the additional collision on the energy loss to the surface can be significant dependent on how inelastic the contact interactions end up being. This

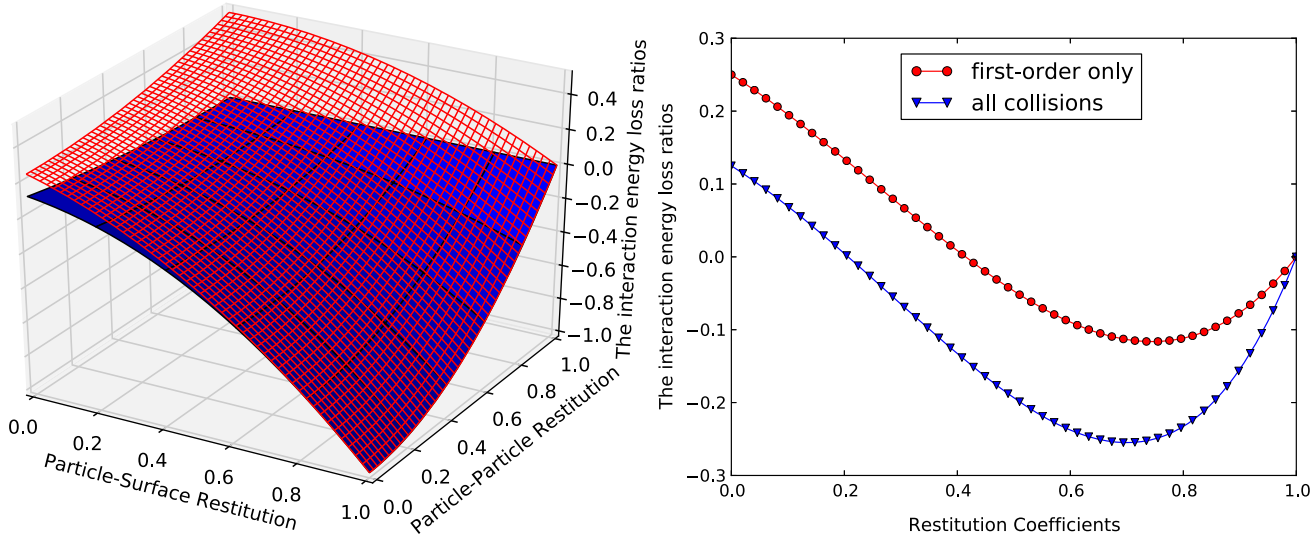

Fig. 4 A comparison of the proportion of energy losses α^* (with all collisions accounted for, and shown in *blue*), and $\overline{\alpha}$ (with only first-order collision effects, and shown in *red*). The special case of equal e_s and e_p values has been presented on the *right* (color figure online)

motivates the idea that for a significant number of repeated collisions, the energetics of a jet of multiple particles can deviate markedly from that of a jet where only first-order collision effects are taken into account. Of course, the total energy available to the surface is due to only one particle surface impact if first-order collisions are taken into account, while in reality there are two particle–surface impacts—which is another aspect of importance in many erosive wear applications. This idea of energy losses due to interacting jets will be re-visited at a later section to investigate the interference effects in a stream of multiple particles.

3 Simulation of system dynamics

A typical system configuration for the numerical simulations have been presented in Fig. 5, where the grid for stress-calculation has been explicitly demarcated. The layer width W was chosen to be wide enough so that edge effects in estimating sub-surface stresses can be neglected. Refer to Fig. 2 for an illustration of handling each individual particle impacts to calculate the stresses. The overall simulation framework can be illustrated starting from a consistent representation of the dynamics of individual particles. Elaborating further on this, consider the system to be made up of N_p particles, where for each individual particle indexed by i, we can write:

$$m_i \frac{d\mathbf{v}_i}{dt} = \sum_{j=1}^{N_s} \overbrace{\mathcal{I}(\mathcal{P}_i, \mathcal{S}_j)}^{\text{check contact}} \underbrace{\left[\mathbf{F}_{ijs,contact}\right]}_{\text{particle–surface}} + \sum_{j\neq i, j=1}^{N_p} \overbrace{\mathcal{I}(\mathcal{P}_i, \mathcal{P}_j)}^{\text{check contact}} \underbrace{\left[\mathbf{F}_{ij,contact}\right]}_{\text{particle–particle}} \tag{38}$$

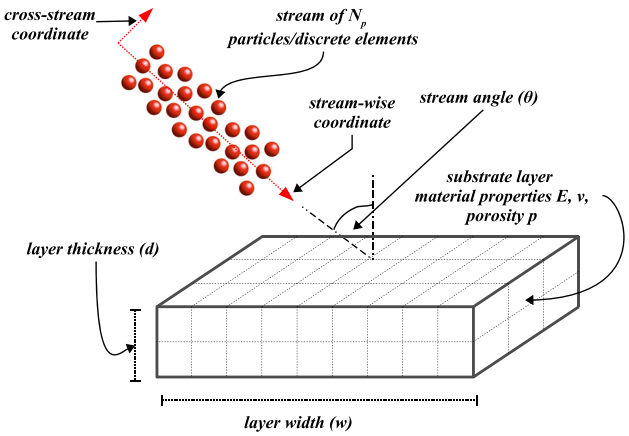

Fig. 5 The typical system configuration for the erosive jet impact that will be considered for the simulation framework and the analysis (color figure online)

$$\frac{d\mathbf{x}_i}{dt} = \mathbf{v}_i \tag{39}$$

where $\mathcal{P}_i$ indicates the i-th particle, and $\mathcal{S}_j$ represents the j-th surface in the computation domain comprising N_s surfaces. The equation has been kept general so that multiple surfaces can be incorporated in the simulation. For the current work, it will be assumed that the contribution of the rotational motion of the individual particles to the overall system dynamics is not significant. This is a reasonable assumption for small particles moving at significantly high translational velocities, whence for any angular motion to have significant impact we should have $\mathcal{O}(\| \boldsymbol{\omega}_i \|) \approx \| \mathbf{v}_i \| / R_i$, which necessitates very high angular velocities. The function $\mathcal{I}(\cdot, \cdot)$ is an indicator function that represents contact check between a pair of particles, or a particle and a surface. For a pair of par-

ticles, this indicator function can be mathematically defined as:

$$\delta_{n,ij} = \|\mathbf{r}_i - \mathbf{r}_j\| - \left(R_i + R_j\right)$$
$$\mathcal{I}(\mathcal{P}_i, \mathcal{P}_j) = \begin{cases} 1 & \text{if } \delta_{n,ij} \leq 0 \text{ (contact)} \\ 0 & \text{if } \delta_{n,ij} > 0 \text{ (no contact)} \end{cases} \tag{40}$$

For a particle–surface contact check, the form of the indicator function remains the same. The only variation is in the evaluation of the contact overlap $\delta_{n,ij}$. For interactions between a spherical particle and a plane surface—which is the application we are interested in here—this can be estimated by considering the plane $\mathcal{S}_j$ to be defined as $a_j x + b_j y + c_j z + d_j = 0$ in three-dimensional Euclidean space, and writing the overlap using the total distance of the center of the sphere from this plane as follows:

$$\delta_{n,ij} = \frac{\|a_j x_i + b_j y_i + c_j z_i + d_j\|}{\sqrt{a_j^2 + b_j^2 + c_j^2}} - R_i$$
$$\mathcal{I}(\mathcal{P}_i, \mathcal{S}_j) = \begin{cases} 1 & \text{if } \delta_{n,ij} \leq 0 \text{ (contact)} \\ 0 & \text{if } \delta_{n,ij} > 0 \text{ (no contact)} \end{cases} \tag{41}$$

Assuming a system of N_p particles, it is evident that a naive implementation of the evaluation of the pairwise contact check $\mathcal{I}(\mathcal{P}_i, \mathcal{P}_j)$ will lead to prohibitively high computational costs, scaling asymptotically with the number of particles as $\mathcal{O}\left(N_p^2\right)$. To deal with this efficiently, it is noted that contact interactions (and other similar short-range interactions) for any particle will be restricted mainly within other neighboring particles in close vicinity. Therefore ideas based on partitioning of particles in the domain, and maintaining a list of close neighbors for each particles can be used to reduce the number of pairwise contact checks, making the computations more efficient. For the current work, a variant of the 'Cell-List' method (also otherwise referred to as the 'Linked-Cell List' method or simply 'Binning' method) is used to create the neighbor list, and the interested reader is referred to Poschel and Schwager [42], Frenkel and Smit [18], and Mattson and Rice [30] for further details. For the simulations, an overall computation domain that is large enough to resolve all the interesting dynamics is binned and tracked throughout the time-steps. Any particle that goes outside of this computation domain is taken out of the time-step calculations.

The time-integration of the motion equations presented in Eqs. (38) and (39) have been performed using the one-step ϕ-type method, with the discretized form of the motion equations derived to be as follows:

$$\mathbf{v}_i^{N+1} - \mathbf{v}_i^N = \frac{\Delta t}{2m_i}\left[\phi \mathbf{F}_i^{N+1} + (1-\phi)\mathbf{F}_i^N\right] \tag{42}$$
$$\mathbf{F}_i^N = \sum_{j=1}^{N_s} \mathcal{I}(\mathcal{P}_i, \mathcal{S}_j)\left[\mathbf{F}_{ijs,contact}\right]^N + \sum_{j\neq i, j=1}^{N_p} \mathcal{I}(\mathcal{P}_i, \mathcal{P}_j)\left[\mathbf{F}_{ij,contact}\right]^N \tag{43}$$
$$\mathbf{x}_i^{N+1} - \mathbf{x}_i^N = \frac{\Delta t}{2}\left[\phi \mathbf{v}_i^{N+1} + (1-\phi)\mathbf{v}_i^N\right] \tag{44}$$

where the superscript N indicates indices of time-steps, $\phi \in [0, 1]$, and for $\phi > 0$ the scheme is implicit, requiring an iterative solution of Eqs. (42) and (44). The discretization of the motion equations could also be performed using other well-known numerical schemes for solutions of ordinary differential equations. However, for the current work, the ϕ-type method was chosen for it's simplicity and ease of implementation. The overall iterative error measure that is used for termination criteria for the time-step iterations is defined as follows:

$$e_{iter} = \sum_i \frac{\|\mathbf{v}_i^{N+1,K+1} - \mathbf{v}_i^{N+1,K}\| + \|\mathbf{x}_i^{N+1,K+1} - \mathbf{x}_i^{N+1,K}\|}{\|\mathbf{v}_i^{N+1,K+1} - \mathbf{v}_i^{N+1,0}\| + \|\mathbf{x}_i^{N+1,K+1} - \mathbf{x}_i^{N+1,0}\|} \tag{45}$$

As a further implementation detail, it must be noted that owing to the initial assumption that the time-step sizes chosen must be larger than the collision duration, it is expected that within a single time-step, upon completion of momentum transfer due to collision, the relative-velocity of approach along the normal direction will either be reversed or be zero. Hence it is advisable to make the contact forces non-zero only when the relative normal-velocities of impact are negative ($v_{c,n}(t) < 0$).

Since this is a system of initial value problems, an initial configuration of particles needs to be specified for the differential equations to be solved. For the system in concern, it requires specifying a set of particles with their initial positions and velocities. This configuration can be generated using a Random Sequential Addition (RSA) method as proposed by Widom [53], and later improved upon by Torquato et al. [47]. The basic operation of the algorithm has been illustrated using a flowchart as in Fig. 6 (on the right). Although other forms of algorithms based on a collide-and-grow type phenomenology also exist (see for example Lubachevsky and Stillinger [29]) for generating particle configurations of higher number densities since our interest is in analyzing loosely flowing particulate streams, for the current application an RSA algorithm was sufficient. The overall algorithmic implementation of the simulation of system dynamics has been illustrated in Algorithm 1. A sample particle ensemble for 10,000 particles in a cuboidal region of dimensions 2.5

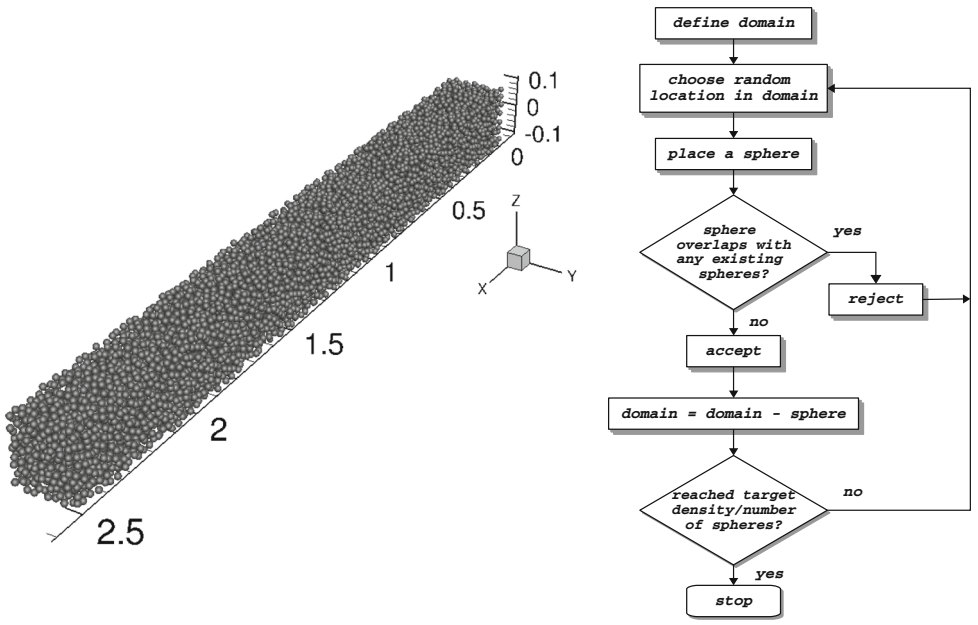

Fig. 6 A representation of a typical mono-disperse particle ensemble created by using a random sequential addition algorithm (*left*), and the corresponding pesudocode representation of the algorithm used to generate such ensembles (*right*)

by 0.2 by 0.2 length units obtained using such an algorithm has been presented in Fig. 6. It is remarked here that a more elaborate arrangement of initializing a configuration of particles can be also implemented to account for, amongst other aspects, the angle of divergence for a diverging stream of particles, as presented in Ciampini et al. [14].

Remark As a further implementation detail, from the pseudocode in Algorithm 1, it is evident that for a large number of particles, and for a very fine mesh, the stress calculation loop can become computationally intensive. However, it is a set of decoupled calculations for each individual grid-point and for each impacting particle. Thus, using linear superposition of stresses, this entire loop can be computed in parallel—with collections of grid points being distributed amongst various processes for stress calculations owing to multiple particle impact at each time-step. The implementation of this, for the present framework, was done using shared memory parallelism via Open-MP in Fortran. This parallel implementation can be used to perform calculations over much finer meshes.

Algorithm 1 *A pseudocode to illustrate the implementation of time-stepping with staggered, iterative updates for integrating particle equations using the one-step trapezoidal scheme as performed in the developed simulation framework.*

evaluate all particle particle contacts
evaluate all particle surface contacts
for $i = 1, N_p$ **do**
  $\mathbf{F}_i^N \leftarrow$ sum of all forces
  $\mathbf{v}_i^N \leftarrow$ store current velocity
  $\mathbf{x}_i^N \leftarrow$ store current position
  set initial guess for velocity $\rightarrow \mathbf{v}_i^{N+1,0}$
  set initial guess for position $\rightarrow \mathbf{x}_i^{N+1,0}$
  update dynamic variables $\mathbf{v}_i, \mathbf{x}_i$
end for
while (*error* $\geq$ *error tolerance*) **do**
  evaluate all particle particle contacts
  evaluate all particle surface contacts
  for $i = 1, N_p$ **do**
    $\mathbf{F}_i^{N+1,K} \leftarrow$ sum of all forces
    $\mathbf{v}_i^{N+1,K+1} = \mathbf{v}_i^N + \frac{\Delta t}{2m_i}\left[\mathbf{F}_i^{N+1,K} + \mathbf{F}_i^N\right]$
    $\mathbf{x}_i^{N+1,K+1} = \mathbf{x}_i^N + \frac{\Delta t}{2}\left[\mathbf{v}_i^{N+1,K+1} + \mathbf{v}_i^N\right]$
    update dynamic variables $\mathbf{v}_i, \mathbf{x}_i$
  end for
  $error = \sum_i \frac{\|\mathbf{v}_i^{N+1,K+1} - \mathbf{v}_i^{N+1,K}\| + \|\mathbf{x}_i^{N+1,K+1} - \mathbf{x}_i^{N+1,K}\|}{\|\mathbf{v}_i^{N+1,K+1} - \mathbf{v}_i^{N+1,0}\| + \|\mathbf{x}_i^{N+1,K+1} - \mathbf{x}_i^{N+1,0}\|}$
end while
for $i = 1, N_p$ **do**
  if (*particle i contacts surface*) **then**
    for $p = 1$, num-grid-points **do**
      $\sigma \leftarrow$ calculate stresses due to contact-force on the surface
      $\sigma_p = \sigma_p + \sigma$
    end for
  end if
end for

4 Numerical examples and analysis

4.1 Stream dynamics and damage accumulation

The values of the various simulation parameters and their ranges that have been used in all the simulation examples presented in this work have been tabulated in Table 1. Wherever

Table 1 Table for the values and ranges for various simulation parameters used for the numerical analysis presented in this work. Stream impingement angle of 0.0 corresponds to stream directed normally to the surface

Parameters	Values/ranges
Jet dimensions	2.5 m × 0.2 m × 0.2 m
Particle radius	0.01 m
Particle density	8500.00 kg m^3
Bulk modulus of material	100.0 GPa
Target to stream distance	0.1–0.4 m
Velocity of stream	80.0 m/s
Porosity of material	0.0–0.5
Number of particles	500–10,000
Stream impingement angle	0.0°–75.0°
Restitution coefficients	0.0–1.0
Friction coefficients	0.0–0.5

necessary, in the figures for the simulation results, specific parameter choices have been highlighted. In order to demonstrate the overall dynamics of the particulate jet as it impacts a surface, successive snapshots of a particulate stream with 10,000 mono-disperse (that is, all particles having the same radius) particles impacting a surface have been presented in Fig. 7. The particular value for particle number-density was chosen so as to demonstrate the dynamics of a relatively high mass flux/density of eroding jets. It is evident from the stream dynamics that the inherent randomness in the configuration of the particles in the stream allows for oblique, non-normal impacts between particles in the stream—originating mainly from the collisions between the particles from the incoming stream, and the particles rebounding from the surface and re-entering the stream. This causes a spread pattern in the particulate stream as is visible in the snap-shots in Fig. 7. The patterns observed are similar in nature to the ones reported experimentally in the work by Cheng et al. [12], for dense, dry, granular jets impacting a circular target. It is noted here however that their experiments involved dense particle jets compacted by repeated tapping, while the ones used in the simulations here are of lower particle volume number density. The corresponding accumulated values of damage within the continuum of the material, as calculated using the model in Sect. 2.5 have also been visualized using successive snapshots during the simulation time presented in Fig. 8. The propagating contours indicating points where damage equivalent stress thresholds are violated, are symmetric as is expected—with some fluctuations appearing from the discrete nature of the particle–surface impacts. It is expected that as the particle number density reduces, there will be reduction in the number interfering collisions, thereby not leading to the formation of a spread pattern like the one shown in Fig. 7. To illustrate this idea, snap-shots of the stream dynamic after identical durations of simulation time for three varying number densities have been presented in Fig. 9. At a lower number density the dynamic particle configuration looks comparable to the ones obtained from computer simulations performed by Ciampini et al. [14].

As the energy imparted onto the target surface is translated into stresses within the material continuum, the microstructure of the material layer will affect the stress levels significantly. For the current work the information on porosity has been incorporated using an effective property based model. The inclusion of the pores weakens the material, and therefore it is expected that stress levels will be higher for more porous materials. To illustrate the effect of porosity in the context of erosive particulate stream impacting a surface, the upper bounds for the material properties were chosen, and a variation of the obtained bulk modulus,shear modulus, and Poisson's ratio for varying porosity levels has been presented in Fig. 10 on the left. The effect of porosity on damage equivalent stress magnitudes has been illustrated by tracking the the damage equivalent stress levels at a point very close to the centerline located across the depth of the material layer, for varying porosity levels. The obtained stress levels have been presented in Fig. 10 on the right. At various locations, while the stress magnitudes will vary depending on proximity to jet centerline, the relative trend with varying porosity was found to be the same.

The angle of impingement of the jet is another important parameter that affects the jet dynamics. In Fig. 11 snapshots of the 10,000-particle jet at identical instants during the simulation have been presented for varying impingement angles. It can be seen that at the region proximal to the surface (that is, for this example, the lower half of the surface) the jet impacts first, causing reflected particles to be pushed into the oncoming stream and thereby causing more collisions in that region. At the distal region (that is, for this example, the upper half of the surface) the particles experience lesser interfering collisions, thereby losing less energy. The extent of the collision zone, and the loads experienced by the surface both therefore become asymmetric, showing a predilection towards the angle of the stream—a fact that is ably supported by a comparison of the damage patterns obtained for a normal and angular (30° and 60°) jets for the same particle number density as presented in Fig. 12. The patterns of the distribution of the damage equivalent stress and evaluated damage correlates well with the observations presented by Oka et al. [39] based on sand blasting experiments on Aluminium surfaces. An exact determination of the eroded area geometry, however, is dependent on the mechanism of wear, and such a quantitative comparison would require much detailed modeling effort in terms of damage evaluation as compared to the simplified approach presented here. It is noted that in all the examples presented here, repeated collisions between particles, and between particle and surface are accounted for.

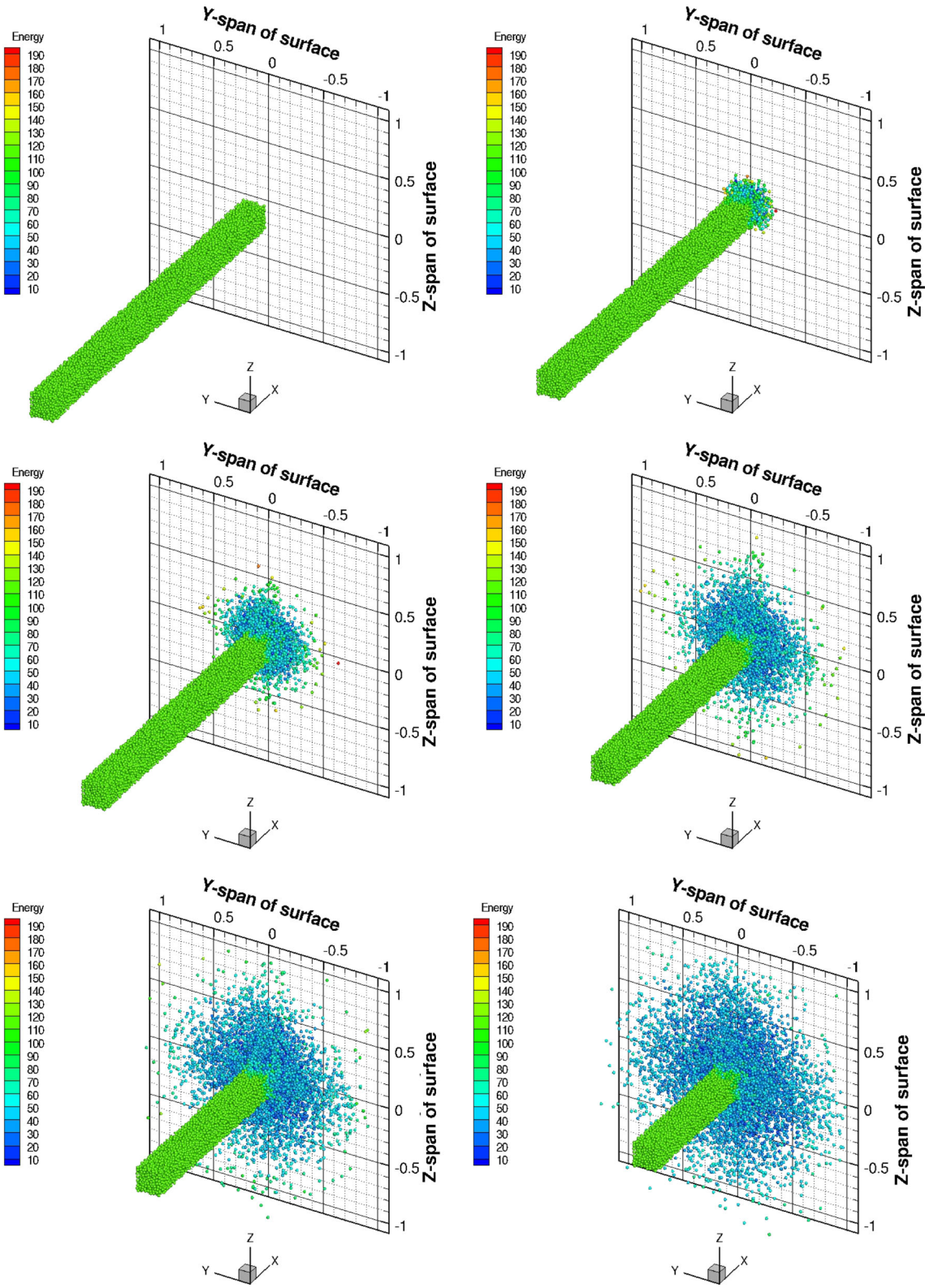

Fig. 7 Snapshots of the dynamics of a stream of 10,000 particles impacting a surface, with restitution coefficient 0.8, and friction coefficient being 0.5. The particles are *colored* by their total energy content (color figure online)

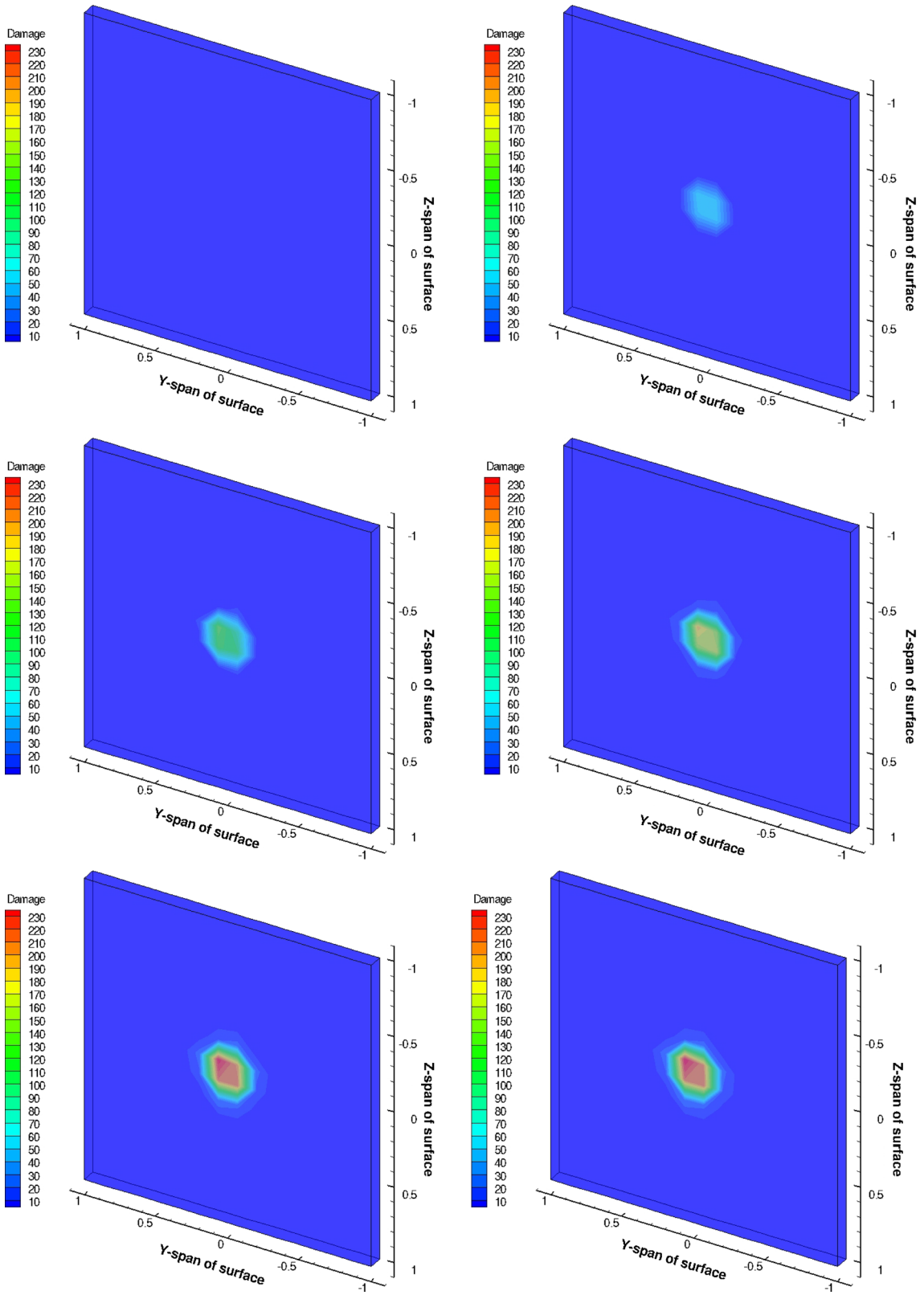

Fig. 8 Snapshots of the evolving contours of surface and sub-surface damage for the impacting jet illustrated in Fig. 7 (color figure online)

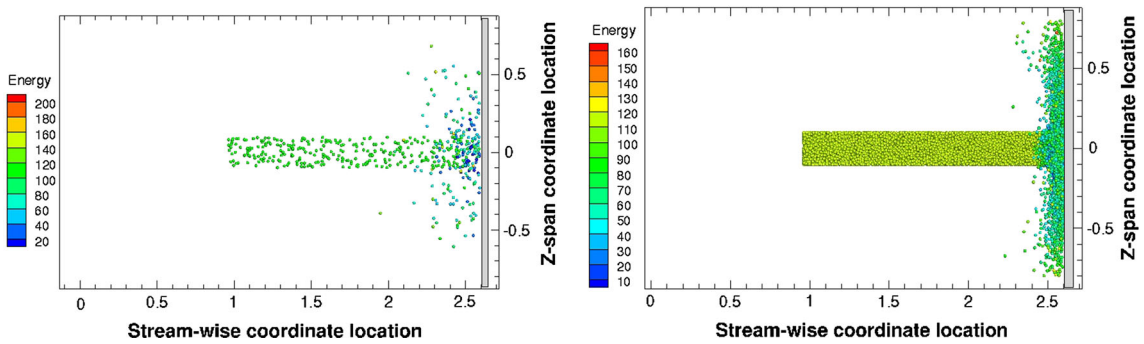

Fig. 9 Typical particle stream trajectories after identical number of simulation time-steps for a jet containing 500 particles (*left*) and that containing 10,000 particles (*right*) (color figure online)

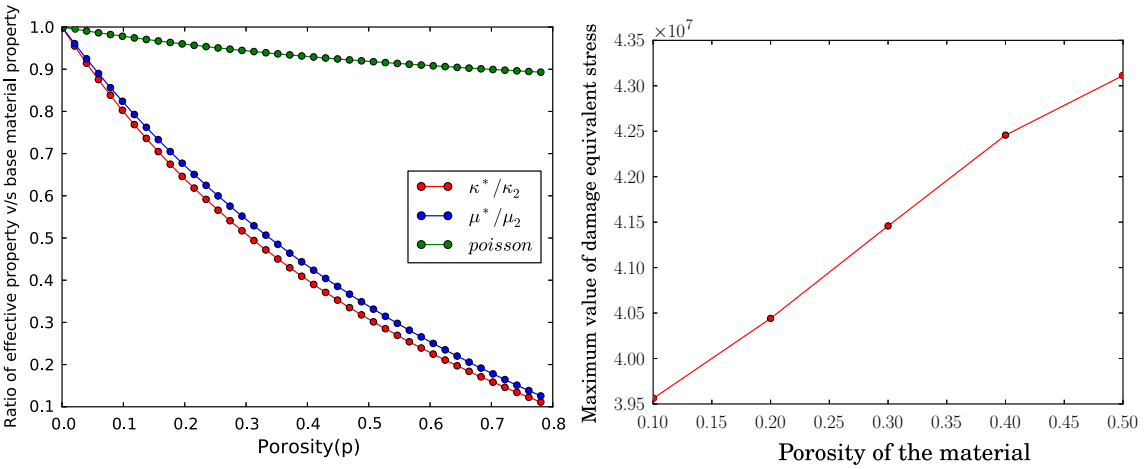

Fig. 10 Sample simulation results illustrating the effect of porosity. The overall material property dependence on porosity as modeled in this work has been shown on the *left*, while the compared maximum damage equivalent stress levels at the centerline, across the depth of the material have been shown on the *right* (color figure online)

4.2 Energetics and interference effects

The specific issue of investigating the interference effects using the framework presented here will now be explored. It is noted that the loads on the surface and the sub-surface stress levels are directly correlated to the energy of particles impacting with the surface. Higher magnitudes of this available energy to the surface leads to greater impact velocities, thereby causing higher impact forces [see Eq. (19)] and larger stresses. A comparison of the time-history of the total energy with which particles impact the surface at all the instances during the entire simulation duration for a particulate jet containing 10,000 particles has been presented for varying restitution coefficient values in Fig. 13. For this particular comparison the friction coefficient was assumed to be zero—so that all the energy losses are only due to inelastic effects during the collision. It is observed that for more elastic collisions (that is, higher values of restitution), the energy available to the surface is substantially less as compared to highly inelastic collisions. This can be explained by the effective shielding of the oncoming particles by the rebounding particles, owing to which lesser proportion of the oncoming particles are able to carry their energy up to the surface for more elastic collisions. As the collisions get more inelastic, the velocities with which oncoming particles are ricocheting away are lesser. These slow moving particles reside in the vicinity of the surface for longer durations and lead to multiple repeated collisions, causing more proportion of the particles' energy to reach the surface. These multiple collisions can be resolved using the simulation framework, which leads to the trends presented in the Fig. 13. Similar conjecture regarding the increased energy transfer at more inelastic collisions have been presented in Gomes-Ferreira et al. [19], where the estimation of fluxes using curve-fitting of obtained simulation data was noted to be inadequate to capture high degrees of interference for highly inelastic collisions. The tail end of the time-history plots for each case in Fig. 13 indicates the stage where all particles in the jet have started moving away from the surface, thereby imparting no more energy to the surface. The corresponding simulations

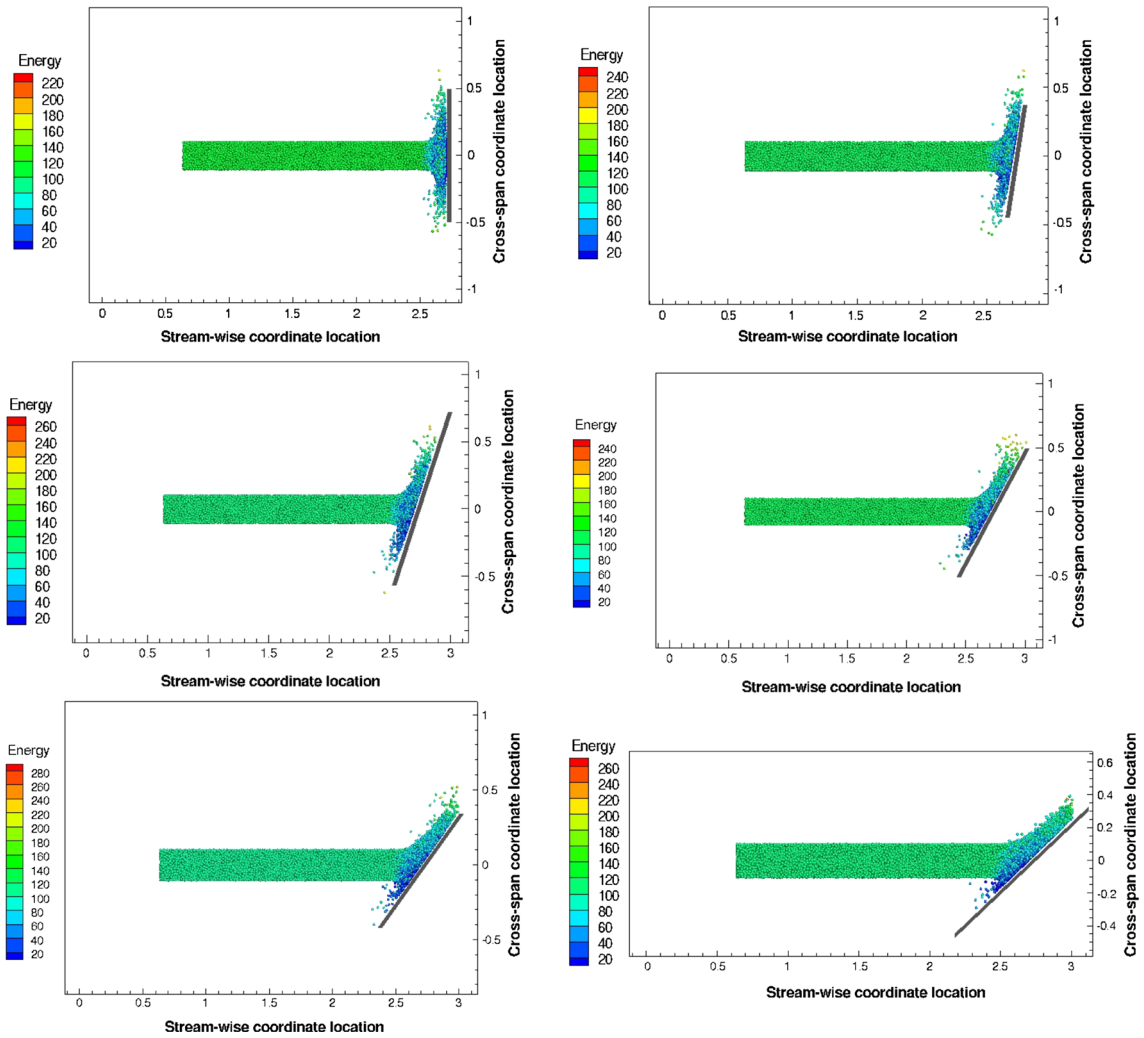

Fig. 11 Snapshots of the lateral view of the spread pattern for a stream containing 10,000 particles impacting a surface oriented at varying angles with respect to the jet impingement direction. All snapshots were taken after identical number of simulation time-steps. The jet impact angles are 0°, 10°, 20°, 30°, 40°, and 50° respectively (from *top* to *bottom* and *left* to *right*) (color figure online)

were re-performed with non-zero friction and the results have been summarized in Fig. 14. The trends with regards to restitution coefficient, and the variation with simulation time are identical as for the frictionless case. The proportion of the energy carried to the surface is reduced however, owing to frictional losses at each collision.

During the course of the simulation the impacting stream dynamics almost attains a quasi-steady state as can be observed from Figs. 13 and 14. Considering the average magnitude of the energy available to the surface during this quasi-steady regime, the overall trend of the variation of the proportion of initial stream energy E_0 that is available to the surface can be quantified with respect to changes in inelasticity and frictional losses during the collisions. For the representative high particle density stream, these trends have been illustrated in Fig. 15. A mild reduction in the available energy is observed in the higher regimes of restitution owing to more elastic collisions between particles causing a greater proportion of the particles to be pushed away from the surface with higher velocities. The energy levels rise significantly thereafter as the collisions get more inelastic.

In order to now present a simple energy-based parameter to capture the trends of interfering collisions, the model problem presented in Sect. 2.6 is referred to. Proceeding similarly as in the two-particle case, let us consider that the system of particles was initiated with a constant initial velocity v_0, and undergoes no interference between oncoming particle stream and reflected particles from the surface. In this case, a set of N_p particles (identical, with mass m) would have arrived at the surface with an energy magnitude $E_0 = \frac{1}{2} N_p m v_0^2$. In the absence of any external forces, the velocities get reduced according to the restitution coefficient, and the particles would rebound with an energy magnitude $E_f = \frac{1}{2} N_p m e^2 v_0^2$. For the overall stream then, the energy

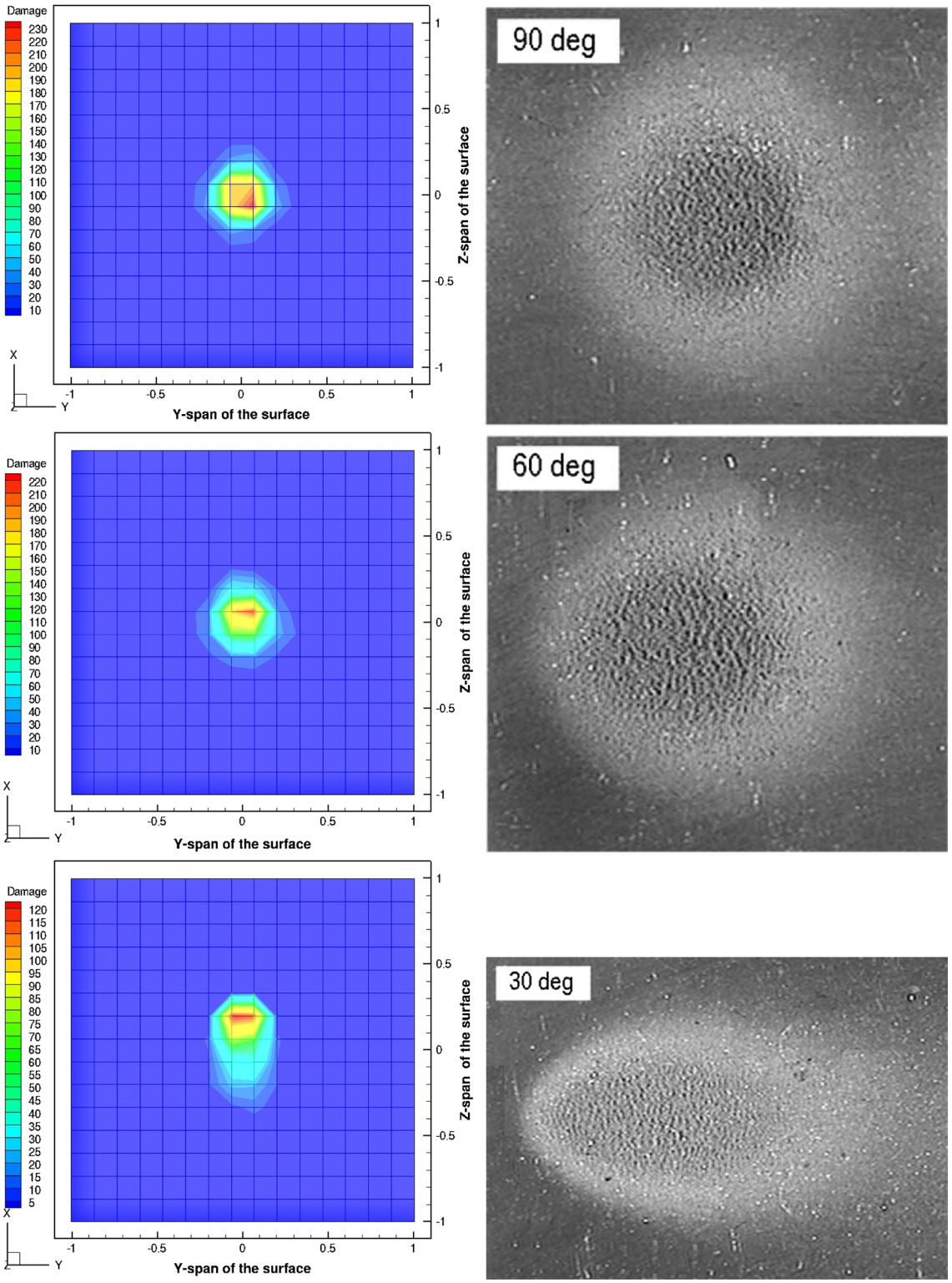

Fig. 12 A comparison of the final damage patterns obtained owing to streams impacting normal to the surface, and angled at 30° to the surface normal. The column on the *right* represent eroded sample images from Oka et al. [39] (figures rotated by 90° counterclockwise as compared to the simulation results on the *left*) (color figure online)

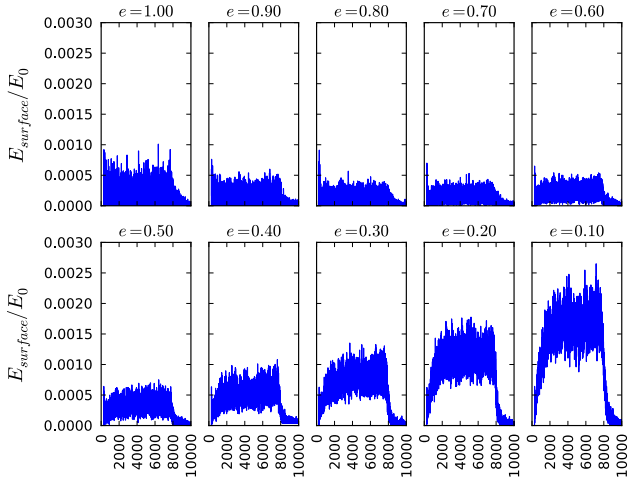

Fig. 13 A comparison of the time-histories of the proportion of total initial particle energy that is available to the surface during the impact of the particle jet for varying restitution coefficient values and for frictionless contacts. The x-axis in each sub-plot denotes the total number of simulation time-steps (color figure online)

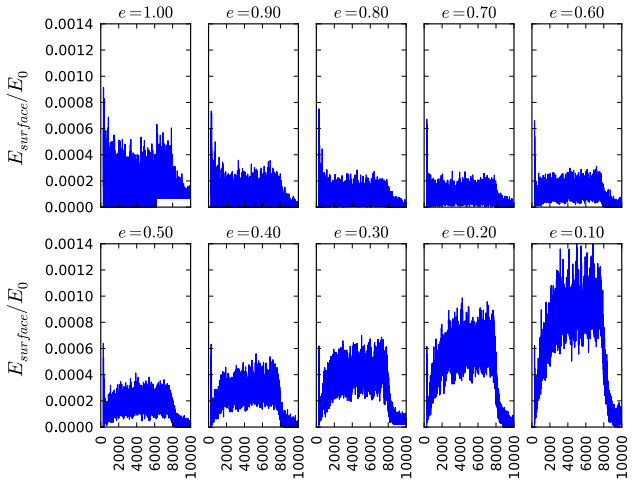

Fig. 14 A comparison of the time-histories of the proportion of total initial particle energy that is available to the surface during the impact of the particle jet for varying restitution coefficient values and for friction coefficient value of 0.4. A general trend of reduced proportion of available energy is observed. The x-axis in each sub-plot denotes the total number of simulation time-steps (color figure online)

difference after all the particles have impacted, given that there is no interference, can be written as:

$$\Delta E_0 = \frac{1}{2}N_p m v_0^2 - \frac{1}{2}N_p m e^2 v_0^2 = \frac{1}{2}N_p m(1-e^2)v_0^2 \qquad (46)$$

Now, interfering collisions between oncoming particles and particles reflected from the surface will lead to the particle velocities being modified, and the energy that the particles carry to the surface as they impact E_{surf} and the total change in energy ΔE will not be the same as mentioned above (recall the two-particle example in Sect. 2.6). Specifically, the inelasticity in the collisions (parametrically represented

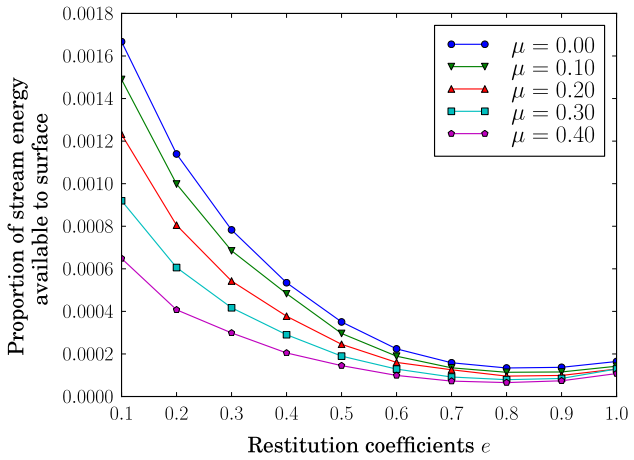

Fig. 15 The combined effect of contact inelasticity (parametrized by restitution coefficient), and frictional effects on the average amount of energy available to the surface during the impact of the jet (color figure online)

through the restitution coefficients), the frictional losses during the collisions, and the fact that the particle surface collisions are no longer going to be head-on, will contribute to this difference in energy loss. Following the example in Sect. 2.6, it seems reasonable to define the following overall system variable to capture the parametric variation of the interference effects:

$$\alpha_{interf} = \frac{\Delta E_0 - \Delta E_{sim}}{E_0} = \frac{E_{f,sim}(N_p, e, \mu, \theta, v_0) - \frac{1}{2}N_p m e^2 v_0^2}{\frac{1}{2}N_p m v_0^2} \qquad (47)$$

In case of no inter-particle interactions, $\alpha_{interf} = 0$ since the energy losses will only be due to particles colliding with the surface. Negative values of α_{interf} corresponds to cases where reflected particles shield and push oncoming particles away with higher velocities. Positive values of α_{interf} correlate with the scenario where slow moving particles, trapped in the proximity of the surface undergo repeated collisions and energy exchange with both the oncoming stream, and the surface. The parametric dependence has been explicitly written out, with $E_{f,sim}$ being the final energy of the system of N_p particles after the simulation over a certain duration is completed. The obtained values of α_{interf} from simulations involving the 10,000-particle jet have been compiled and presented for varying values of friction and restitution in Fig. 16.

The analysis presented thus far is based on a normally impacting stream. The effect of the stream angle on the variation of available energy to the surface can be discussed in a similar manner—that is, considering the average energy available to the surface during the quasi-steady regime of the impact dynamics, and comparing its magnitude with the

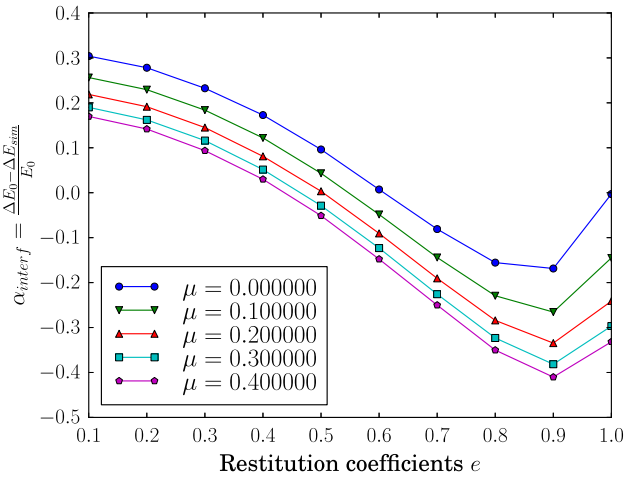

Fig. 16 The obtained variation in the energy based interference parameter α_{interf} with respect to restitution coefficient and friction, obtained from simulation data for impact of the 10,000-particle jet with a surface at normal incidence (color figure online)

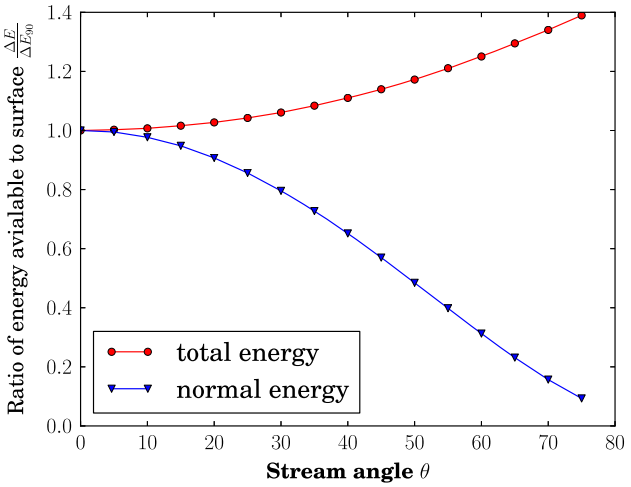

Fig. 17 The variation of the available energy to the surface as the jet impingement angle varies. All values have been non-dimensionalised using the corresponding values for a normally impacting jet (color figure online)

energy available during a normal impact. This ratio of total impact energy is compared with stream angles for the representative 10,000 particle jet in Fig. 17. The figure also compares the variation of the total available energy that is normal to the surface. In general, the erosion rate is proportional to the energy of the impacting particles as has been presented by Finnie [17], Shipway and Hutchings [45], Ramanujam and Nakamura [43], and also in the analysis presented by Ciampini et al. [14] and [13]. For initial phases of the erosion, or for brittle erosive wear, the normal impact loading will be dominant as has been shown for example by Ramanujam and Nakamura [43]. For an actual comparison of the reported trend in Fig. 17, the particular example of erosion of thermal barrier coatings and their dependence on impact angle as reported by Nicholls et al. [37] was used. Thermal barrier coating erosion is pre-dominantly brittle in nature, thereby leading to the normal energy being the dominant factor in erosion process—and the trend reported in Nicholls et al. [37] for APS and EB-PVD coating wear correlates very well with the trend reported in Fig. 17. There could be more complicated mechanisms however, wherein the total energy, and its distribution amongst normal and tangential components will govern the overall erosive behavior. For a mechanism that incorporates a combination of normal and tangential energies, the erosive wear will be maximized therefore at some intermediate angle of impingement—which is what typical observations of erosion rate in test facilities indicate. For further details on impact angle dependence, the interested reader is referred to the discussion presented by Oka et al. [40].

In the work presented by Anand et al. [1] (see also Burzynski and Papini [7]) an exponential dependence of erosion rate on flux of the eroding particles was presented—the general form of which is as follows:

$$\log\left(\frac{e_w}{e_0}\right) = -C_e \Phi \tag{48}$$

where e_w is the erosive wear due to the jet, e_0 is the wear assuming no interference, Φ is the flux, and C_e is a parameter that includes the effect of particle size, initial velocities and other jet parameters. Their expression was derived using assumptions of uniform distribution of velocities and particle locations, which is also true for the numerical examples presented herein. They further assumed that incident particles colliding with rebounding particles once are thereafter removed from the stream. If it is assumed, as mentioned earlier, that the erosive wear is proportional to the energy available to the surface, then the exponential variation should also be true for the variation of this energy—that is, $E_{surf} = \exp(-\overline{C_e}\Phi)$. The available energy for varying particle densities (which in turn denotes varying fluxes), has been compared without any assumption on collisions between incident and rebounding particles, and the obtained trend is compared and fitted with an exponential curve. The results for this analysis for an intermediate collision restitution coefficient value of 0.8 have been presented in Fig. 18. The overall behavior for a broad range of particle numbers is exponential—as is predicted also by Anand et al. This confirms consistency of the simulation calculations. Furthermore, it predicts that the behavior at low particle number densities is more consistently explained using an exponential curve, while behavior at high number densities starts deviating from exponential. This is because at these high particle numbers, the repeated collisions between oncoming and rebounding particles become very significant—thereby causing the latter assumption in the model presented in Eq. (48) to be insufficient for this regime. Since the original set-up for

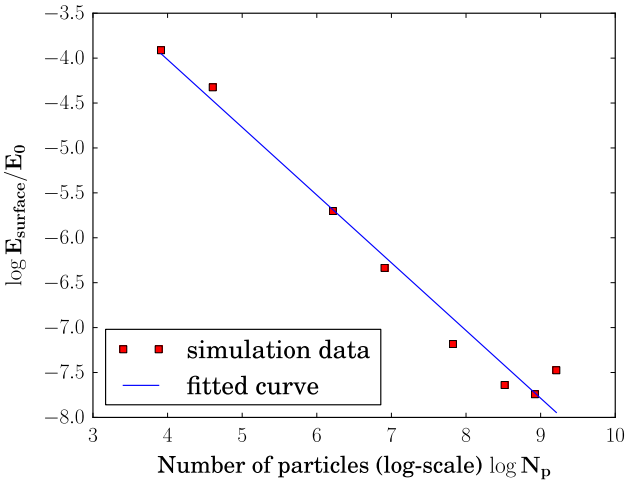

Fig. 18 Comparison of the variation of the proportion of total initial particle energy available to the surface with variation in number of particles. Since the particles are all assumed to be of the same radii (that is, mono-disperse), this corresponds to the total varying eroding particle flux during the fixed duration of the simulation time (color figure online)

the model was for normal impacts, only the normal impact simulation data have been compared here.

5 Concluding remarks

A numerical model based on fully three-dimensional neighbor-list collision driven discrete element method for analysis of the dynamics of a granular jet impacting a surface was presented. The particle energies were translated into sub-surface stresses in the material using a simple particle–continuum interaction based on semi-analytical solutions of stresses due to point loads on an elastic half-space. The simulation was constructed so as to specifically track the information on energy transfer due to repeated inter-particle and particle–surface collision. The framework therefore is general purpose and allows for (1) detailed resolution of interference due to collisions, (2) visualization of sub-surface stress distribution and damage evolution dynamically simultaneously with the jet impact, and (3) retains all the major system parameters which have been reported in previous studies to be of significant importance.

Detailed numerical examples were presented to demonstrate the efficacy of the simulations in predicting typical particle stream trajectory, typical stress levels and damage patterns for the material. The simulations were also used for obtaining detailed insights into the mechanics of the interfering collisions and their effect on the energy carried by the particle unto the surface. A few particular remarks to summarize some of the specific aspects can be outlined as follows:

– The interfering collisions and the inherent randomness in the spatial configuration of the particles in the incoming jet lead to a randomness in impact velocities and angles for the particles striking the surface. For highly inelastic collisions, the particles rebound with slow velocities and can remain in the proximity of the surface for longer durations, thereby causing more frequent collisions with the incoming stream and lead to higher available energy to the surface. Higher particle number densities also cause higher extents of repeated collisions, and the variations in the energy carried up to the surface for these deviate from the exponential trend observed in existing literature. Therefore, for high values of particle number densities, the assumption of considering first-order collisions only may not be sufficient to capture the dynamics of the impacting jet.
– Wherever appropriate, the results and the trends obtained from the numerical simulations were compared with available data in the literature. Through repeated numerical experimentation, the reported trends were found to be generic and robust.
– For comparison with available experimental studies on erosive wear, the jet dimensions, jet velocity, particle size, and properties were chosen so as to attain an eroding particle mass flux which is within the range of what these experimental studies employ. The eroding particle flux scales linearly with number of particles, cubically with particle size, and inverse cubically with jet dimensions. These factors, led to a choice of number of particles that are lower than what is considered in experimental studies on dense granular jets. We remark here that the objective of this paper was not to address flows of granular jets of high number densities, and also the bigger particle sizes used did not alter the observations on stress and damage patterns on the material surface (as evident in Fig. 12). Furthermore, as far as the capabilities of the framework are concerned, the number of particles is not a limitation, and the framework can be used for higher number of particles, or denser granular jets.
– In all the example simulations presented, the restitution and friction coefficients for inter-particle and particle–surface collisions were assumed to be equal. This was done just for convenience of presenting the relevant information for discussing details about the mechanics of the interference and its role in erosive wear. This was not owing to any limitation of the framework—these sets of parameters can, if required, be assigned different values and the corresponding system behavior can be obtained.
– Since a general purpose parametric test on system behavior to obtain a correlative equation for predicting erosive wear was not the objective of the current study, there are a few parameters whose variations have not been considered explicitly in the examples provided. These include the stream-target stand-off distance, the input stream velocity, and the particle radius values. A more general pur-

pose system parametric analysis (like the one presented by Ciampini et al. [13] for erosive granular jets, or by Waitukaitis et al. [51] for cohesive, free-falling, particulate streams) could be easily undertaken now—given the simulation framework. Furthermore, information about the surface material micro-structure could be added to the overall set of system parameters whose influence on total erosive damage can be tested.

The ability to handle the interfering, repeated collisional interactions between particles, using the momentum-balance formulation for handling contacts allows us to resolve the complex interactions within the jet, close to the target surface. Recent studies on granular jets—for example by Huang et al. [25] and Muller et al. [32]—discuss the role of the collisional interactions in the context of formulating a continuum flow description for such jets. Exploring the utility of the collision driven particle dynamics framework devised here in providing further insights into such aspects of granular flow physics is an area of continuing and future research for the authors.

Acknowledgments This work was partly supported by Siemens Energy, and the authors would like to thank them for their support. The work has not been published in any other journal prior to this. There were no study participants involved in this work, as the work was purely computational. The authors also declare that they have no conflict of interest.

Appendix: Stresses due to point loadings

For completeness of presentation, we outline here the expressions for the stresses due to point normal and point tangential loading which have been employed for the sub-surface stress calculations for the particle jet impacting the porous material layer. In the following, it is assumed that the loading acts on a surface located along the x–y plane—at $z = 0$. The point where the load is applied is assumed to be the origin. For any other loading point, simple coordinate transformations need to be employed. Assuming that a normal loading of magnitude F_N is applied along the z direction, the stresses on the surface, and sub-surface is given in cylindrical polar coordinates as follows:

$$\sigma_{rr} = \frac{F_N}{2\pi}\left[(1-2\nu)\left(\frac{1}{r^2} - \frac{z}{\rho r^2}\right) - \frac{3zr^2}{\rho^5}\right] \tag{49}$$

$$\sigma_{\theta\theta} = -\frac{F_N}{2\pi}(1-2\nu)\left[\frac{1}{r^2} - \frac{z}{\rho r^2} - \frac{z}{\rho^3}\right] \tag{50}$$

$$\sigma_{zz} = -\frac{3F_N}{2\pi}\frac{z^3}{\rho^5} \tag{51}$$

$$\sigma_{rz} = -\frac{3F_N}{2\pi}\frac{rz^2}{\rho^5}, \sigma_{\theta z} = \sigma_{\theta r} = 0 \tag{52}$$

where $z \geq 0$, $r^2 = x^2 + y^2$, and $\rho^2 = x^2 + y^2 + z^2$. The expressions are radially symmetric for a single point loading along the loading axis. Corresponding expressions for stresses due to a tangential loading of magnitude F_X applied along the positive x direction can be written as follows:

$$\sigma_{xx} = \frac{F_X}{2\pi}\left[-\frac{3x^3}{\rho^5} + (1-2\nu)\left\{\frac{x}{\rho^3} - \frac{3x}{\rho(\rho+z)^2} + \frac{x^3}{\rho^3(\rho+z)^2} + \frac{2x^3}{\rho^2(\rho+z)^3}\right\}\right] \tag{53}$$

$$\sigma_{yy} = \frac{F_X}{2\pi}\left[-\frac{3xy^2}{\rho^5} + (1-2\nu)\left\{\frac{x}{\rho^3} - \frac{x}{\rho(\rho+z)^2} + \frac{xy^2}{\rho^3(\rho+z)^2} + \frac{2xy^2}{\rho^2(\rho+z)^3}\right\}\right] \tag{54}$$

$$\sigma_{xy} = \frac{F_X}{2\pi}\left[-\frac{3x^2y}{\rho^5} + (1-2\nu)\left\{-\frac{y}{\rho(\rho+z)^2} + \frac{x^2y}{\rho^3(\rho+z)^2} + \frac{2x^2y}{\rho^2(\rho+z)^3}\right\}\right] \tag{55}$$

$$\sigma_{zz} = \frac{F_X}{2\pi}\left[-\frac{3xz^2}{\rho^5}\right] \tag{56}$$

$$\sigma_{yz} = \frac{F_X}{2\pi}\left[-\frac{3xyz}{\rho^5}\right] \tag{57}$$

$$\sigma_{zx} = \frac{F_X}{2\pi}\left[-\frac{3x^2z}{\rho^5}\right] \tag{58}$$

The expressions for point loading along y direction can be obtained from the above by simply interchanging x and y.

References

1. Anand, K., Hovis, S.K., Conrad, H., Scattergood, R.O.: Flux effects in solid particle erosion. Wear **118**(2), 243–257 (1987)
2. Andrews, D.R., Horsfield, N.: Particle collisions in the vicinity of an eroding surface. J. Phys. D Appl. Phys. **16**(4), 525–538 (1983)
3. Arbelaez, D., Zohdi, T.I., Dornfeld, D.A.: Modeling and simulation of material removal with particulate flows. Comput. Mech. **42**(5), 749–759 (2008)
4. Arbelaez, D., Zohdi, T.I., Dornfeld, D.A.: On impinging near-field granular jets. Int. J. Numer. Methods Eng. **80**(6–7), 815–845 (2009)
5. Bitter, J.G.A.: A study of erosion phenomena. Part I. Wear **6**(1), 5–21 (1963)
6. Brilliantov, N.V., Spahn, F., Hertzsch, J.M., Thorsten, P.: Model for collisions in granular gases. Phys. Rev. E **53**(5), 5382–5392 (1996)
7. Burzynski, T., Papini, M.: Analytical models of the interference between incident and rebounding particles within an abrasive jet: comparison with computer simulation. Wear **263**(7–12), 1593–1601 (2007)
8. Burzynski, T., Papini, M.: Analytical model of particle interference effects in divergent erosive jets. Tribol. Int. **43**(3), 554–567 (2010)
9. Camacho, G.T., Ortiz, M.: Computational modelling of impact damage in brittle materials. Int. J. Solids Struct. **33**(2), 2899–2938 (1996)

10. Chaboche, J.L.: Continuum damage mechanics. J. Appl. Mech. **55**(1), 59–64 (1988)
11. Chen, X., Wang, R., Yao, N., Evans, A.G., Hutchinson, J.W., Bruce, R.W.: Foreign object damage in a thermal barrier system: mechanisms and simulations. Mater. Sci. Eng. A **352**(1–2), 221–231 (2003)
12. Cheng, X., Varas, G., Citron, D., Jaeger, H., Nagel, S.: Collective behavior in a granular jet: emergence of a liquid with zero surface tension. Phys. Rev. Lett. **99**(18), 188001 (2007)
13. Ciampini, D., Spelt, J.K., Papini, M.: Simulation of interference effects in particle streams following impact with a flat surface. Part I. Theory and analysis. Wear **254**(3–4), 237–249 (2003)
14. Ciampini, D., Spelt, J.K., Papini, M.: Simulation of interference effects in particle streams following impact with a flat surface part II. Parametric study and implications for erosion testing and blast cleaning. Wear **254**, 250–264 (2003)
15. Cundall, P.A., Strack, O.D.L.: A discrete numerical model for granular assemblies. Géotechnique **29**(1), 47–65 (1979)
16. Duran, J.: Sands, Powders, and Grains: An Introduction to the Physics of Granular Materials. Springer, New York (2000)
17. Finnie, I.: Erosion of surfaces by solid particles. Wear **3**, 87–103 (1960)
18. Frenkel, D., Smit, B.: Understanding Molecular Simulation: From Algorithms to Applications. Academic Press (2001)
19. Gomes-Ferreira, C., Ciampini, D., Papini, M.: The effect of interparticle collisions in erosive streams on the distribution of energy flux incident to a flat surface. Tribol. Int. **37**(10), 791–807 (2004)
20. Haff, P.K., Werner, B.T.: Computer simulation of the mechanical sorting of grains. Powder Technol. **48**(3), 239–245 (1986)
21. Hamilton, G.M.: Explicit equations for the stresses beneath a sliding spherical contact. Proc. Inst. Mech. Eng. C J. Mech. Eng. Sci. **197**, 53–59 (1983)
22. Hashin, Z., Shtrikman, S.: A variational approach to the theory of the effective magnetic permeability of multiphase materials. J. Appl. Phys. **33**(10), 3125–3131 (1962)
23. Hashin, Z., Shtrikman, S.: A variational approach to the theory of the elastic behaviour of multiphase materials. J. Mech. Phys. Solids **11**(2), 127–140 (1963)
24. Hertz, H.: Miscellaneous Papers. Macmillan, New York (1896)
25. Huang, Y.J., Chan, C.K., Zamankhan, P.: Granular jet impingement on a fixed target. Phys. Rev. E **82**(3), 031307 (2010)
26. Hutchings, I.M., Winter, R.E., Field, J.E.: Solid particle erosion of metals: the removal of surface material by spherical projectiles. Proc. R. Soc. Lond. Ser. A Math. Phys. Sci. **348**(1654), 379–392 (1976)
27. Johnson, K.L.: Contact Mechanics. Cambridge University Press, Cambridge (1987)
28. Lemaitre, J., Desmorat, R.: Engineering Damage Mechanics: Ductile, Creep, Fatigue and Brittle Failures. Springer, Berlin (2005)
29. Lubachevsky, B.D., Stillinger, F.H.: Geometric properties of random disk packings. J. Stat. Phys. **60**(5), 561–583 (1990)
30. Mattson, W., Rice, B.M.: Near-neighbor calculations using a modified cell-linked list method. Comput. Phys. Commun. **119**(2–3), 135–148 (1999)
31. Mindlin, R.D.: Compliance of elastic bodies in contact. J. Appl. Mech. **16**, 259–268 (1949)
32. Müller, P., Formella, A., Pöschel, T.: Granular jet impact: probing the ideal fluid description. J. Fluid Mech. **751**, 601–626 (2014)
33. Müller, P., Pöschel, T.: Collision of viscoelastic spheres: compact expressions for the coefficient of normal restitution. Phys. Rev. E **84**(2), 021302 (2011)
34. Müller, P., Pöschel, T.: Two-ball problem revisited: limitations of event-driven modeling. Phys. Rev. E **83**(4), 041304 (2011)
35. Müller, P., Pöschel, T.: Event-driven molecular dynamics of soft particles. Phys. Rev. E **87**(3), 033301 (2013)
36. Murty, K.G.: Linear Complementarity, Linear and Nonlinear Programming. Heldermann, Berlin (1988)
37. Nicholls, J.R., Jaslier, Y., Rickerby, D.S.: Erosion and foreign object damage of thermal barrier coatings. Mater. Sci. Forum **251–254**, 935–948 (1997)
38. Oden, J.T., Pires, E.B.: Nonlocal and nonlinear friction laws and variational principles for contact problems in elasticity. J. Appl. Mech. **50**, 67–76 (1983)
39. Oka, Y.I., Nishimura, M., Nagahashi, K., Matsumura, M.: Control and evaluation of particle impact conditions in a sand erosion test facility. Wear **250**(1–12), 736–743 (2001)
40. Oka, Y.I., Okamura, K., Yoshida, T.: Practical estimation of erosion damage caused by solid particle impact. Wear **259**(1–6), 95–101 (2005)
41. Plantard, G., Papini, M.: Mechanical and electrical behaviors of polymer particles. Experimental study of the contact area between two particles. Experimental validation of a numerical model. Granul. Matter **7**(1), 1–12 (2005)
42. Pöschel, T., Schwager, T.: Computational Granular Dynamics: Models and Algorithms. Springer, Berlin (2005)
43. Ramanujam, N., Nakamura, T.: Erosion mechanisms of thermally sprayed coatings with multiple phases. Surf. Coat. Technol. **204**(1–2), 42–53 (2009)
44. Shäfer, J., Dippel, S., Wolf, D.E.: Force schemes in simulations of granular materials. J. Phys. I **6**(1), 5–20 (1996)
45. Shipway, P.H., Hutchings, I.M.: A method for optimizing the particle flux in erosion testing with a gas-blast apparatus. Wear **174**(1–2), 169–175 (1994)
46. Stewart, D.E.: Rigid-body dynamics with friction and impact. SIAM Rev. **42**(1), 3–39 (2000)
47. Torquato, S., Uche, O., Stillinger, F.: Random sequential addition of hard spheres in high Euclidean dimensions. Phys. Rev. E **74**(6), 1–16 (2006)
48. Uuemois, H., Kleis, I.: A critical analysis of erosion problems which have been little studied. Wear **31**, 359–371 (1975)
49. Vu-Quoc, L., Lesburg, L., Zhang, X.: An accurate tangential forcedisplacement model for granular-flow simulations: contacting spheres with plastic deformation, force-driven formulation. J. Comput. Phys. **196**(1), 298–326 (2004)
50. Vu-Quoc, L., Zhang, X.: An accurate and effcient tangential force-displacement model for elastic frictional contact in particle flow simulations. Mech. Mater. **31**(4), 235–269 (1999)
51. Waitukaitis, S.R., Grütjen, H.F., Royer, J.R., Jaeger, H.M.: Droplet and cluster formation in freely falling granular streams. Phys. Rev. E **83**(5), 051302 (2011)
52. Walton, O.R., Braun, R.L.: Viscosity, granular temperature, and stress calculations for shearing assemblies of inelastic frictional disks. J. Rheol. **30**(5), 949–980 (1986)
53. Widom, B.: Random sequential addition of hard spheres to a volume. J. Chem. Phys. **44**(10), 3888 (1966)
54. Wriggers, P., Zavarise, G.: Computational Contact Mechanics. Springer, Berlin (2002)
55. Zhang, X., Vu-Quoc, L.: An accurate elasto-plastic frictional tangential force displacement model for granular-flow simulations: displacement-driven formulation. J. Comput. Phys. **225**(1), 730–752 (2007)
56. Zohdi, T.I.: Bounding envelopes in multiphase material design. J. Elast. **66**(1), 47–62 (2002)
57. Zohdi, T.I.: On the tailoring of microstructures for prescribed effective properties. Int. J. Fract. **118**(4), 89–94 (2002)
58. Zohdi, T.I.: An introduction to modeling and simulation of particulate flows. In: Computational Science and Engineering, vol 4. Siam, Philadelphia (2007)
59. Zohdi, T.I.: On the dynamics of charged electromagnetic particulate jets. Arch. Comput. Methods Eng. **17**(2), 109–135 (2010)